Copy No. 10

NASA PROJECT APOLLO WORKING PAPER NO. 1077

THE METEOROID ENVIRONMENT AND STRUCTURAL RELIABILITY

RECEIVED
AUG 1970
NASA STI FACILITY
INPUT BRANCH

FACILITY FORM 602

N70-35729
(ACCESSION NUMBER)
(THRU)
73
(PAGES)
1
(CODE)
TMX 65034
(NASA CR OR TMX OR AD NUMBER)
30
(CATEGORY)

[redacted]

NATIONAL AERONAUTICS AND SPACE ADMINISTRATION
MANNED SPACECRAFT CENTER
Houston, Texas

June 12, 1963

Reproduced by
NATIONAL TECHNICAL
INFORMATION SERVICE
Springfield, Va 22151

NASA PROJECT APOLLO WORKING PAPER NO. 1077

THE METEOROID ENVIRONMENT AND STRUCTURAL RELIABILITY

Prepared by: Burton G. Cour-Palais

Burton G. Cour-Palais
AST, Flight Systems

Authorized for Distribution:

Maxime A. Faget
Assistant Director
for Engineering and Development

NATIONAL AERONAUTICS AND SPACE ADMINISTRATION

MANNED SPACECRAFT CENTER

HOUSTON, TEXAS

JUNE 12, 1963

TABLE OF CONTENTS

Section		Page
1.0	INTRODUCTION	1
	SYMBOLS	2
2.0	METEOR THEORY	4
	2.1 Meteor Magnitude	4
	2.2 The Relationship Between Meteor Flux and Visual Magnitude	5
	2.3 The Correlation of Meteor Mass and Flux	7
	2.4 Meteor Velocity	11
	2.5 The Density of Meteoroids	13
	2.6 The Distribution of Meteoroid Orbits	15
3.0	HIGH VELOCITY IMPACT ON METALLIC TARGETS	15
	3.1 Semi-Infinite Targets	16
	3.2 Penetration Formulas for Semi-Infinite Targets	17
	3.3 Double-Sheet Thin Metallic Targets	19
	3.4 Applicability of Penetration Equations to Finite Targets	21
	3.5 The Penetrating Meteoroid Flux	23
4.0	PROBABILITY OF PENETRATION	24
5.0	RELIABILITY AND CONFIDENCE LEVEL	27
6.0	RELIABILITY – EQUIVALENT SKIN THICKNESS RELATIONSHIPS	29
A.1	MSC DESIGN ENVIRONMENTS	30
A.2	CALCULATION OF P_o AND RELIABILITY, R	32
A.3	DESIGNING TO A GIVEN P_o OR R	34
	A.3.1 Based on $P_o = 0.99$	34
	A.3.2 Based on R = 0.99 and C = 97.5%	35
	A.3.3 Designing to a controlled number of penetrations	36
B.1	MATERIAL COMPARISON	38
	B.1.1 Sonic Velocity in Structural Materials	38
B.2	SINGLE THICKNESS AND WEIGHT RELATIVE TO ALUMINUM	38

TABLE OF CONTENTS - Concluded

Section		Page
	B.2.1 Summers' Equation	38
	B.2.2 Bjork's Equation	39
	REFERENCES	40

LIST OF TABLES

Table		Page
1	PENETRATION EFFICIENCY FACTORS FOR DOUBLE-SHEET STRUCTURAL CONFIGURATIONS	42
2	PROBABILITIES OF EXACTLY AND NOT EXCEEDING r EVENTS	43

LIST OF FIGURES

Figure		Page
1	Flux vs magnitude	44
2	Typical light curves	45
3	Flux vs mass	46
4	Height vs meteor mass	47
5	Flux-mass variation with altitude based on dust-belt concept	48
6	Normalized radio meteor velocity distributions	49
7	Normalized distribution of photographic meteor entry velocities	50
8	Average velocity, V_α vs M_v, based on McCrosky's 2433 photographic meteors	51
9	Velocity vs magnitude	52
10	Basic regions of impact as determined for tungsten-carbide spheres impacting lead targets	53
11	Penetration parameters vs impact velocity for aluminum alloy target and projectile	54
12	Penetration parameter vs impact velocity for steel target and projectile	55
13	Penetration parameter vs velocity for finite double-sheet targets	56
14	N_p vs $\bar{t}$ for aluminum	57
15	Probability histogram for np = 5	58
16	Failure rate vs np for 97.5% area	59
17	Reliability factor R as a function of confidence level	60
18	np as a function of $\bar{t}$ based on Summers' equation	61

LIST OF FIGURES - Concluded

Figure		Page
19	np as a function of $\bar{t}$ based on Bjork's equation	62
20	R vs np as a function of confidence level	63
21	Probability P_o vs np with corresponding confidence level	64
22	Probability P_o vs np with corresponding confidence level	65
23	Probability of no more than r events vs np	66
24	$A.\tau$ vs $\bar{t}$ for P = 0.99 of no more than X events	67
25	A vs $\bar{t}$ for P = 0.99 of no more than X events in τ days	68

THE METEOROID ENVIRONMENT AND STRUCTURAL RELIABILITY

1.0 INTRODUCTION

Primarily as a result of the weight limitations on Apollo, a comprehensive survey of the majority of all the articles ever published on meteors, by competent authorities in the field, was undertaken in an attempt to establish the validity of the 1957 Whipple environmental model. This period of review culminated in a visit to the Harvard College Observatory and the Smithsonian Institution Astrophysical Observatory for consultations with Drs. Whipple, McCrosky, Cook, Jacchia, Hawkins, and Southworth.

As the result of all this activity, it was possible to redefine the meteoroid environment based on fact tempered with the respected opinions of the above named experts. The new environment, defined in this paper, was compiled by the Apollo management and support groups as an interim revision. Further revision is inevitable as the data from current and proposed meteoroid sampling programs come to hand.

The position regarding penetration theories has not altered much in the interim between the Apollo study phases and the present time. There is still no concrete proof that Bjork's theoretically deduced equation is any more valid than the empirical Summers-Charters equation at velocities within the meteoric range. The promise of really high-speed impact devices, with controllable masses and velocities, has not materialized to date, hence the solution of this vexing problem has been delayed.

This paper attempts to lay the foundations of a clearer understanding of the problem facing those who have to design for a seemingly nebulous environment. Only those factors truly important in this regard have been included in the appropriate sections dealing with the whole story.

The appendix contains worked examples on the evaluation and design of structure for both the no penetration and the controlled penetration cases. Material selection is dealt with purely from the standpoint of the two penetration theories considered in this paper.

It has not been possible to include any data specifically pertinent to nonmetallic materials under impact. Current practice has been to assume that the results obtained for metallic targets are applicable. Another omission is the subject of micro-meteoroid erosion and it is hoped that a future paper will rectify these shortcomings.

SYMBOLS

A	Area, sq. meter or sq. ft.
a	A constant
C	Confidence level
C_t	Sonic velocity in target material, km per sec
d	Diameter of projectile, cm
F	True failure rate
$\overline{F}$	Most probable failure rate
I	Luminous flux, visual ergs per sec
K	Penetration resistance efficiency factor; a constant
k	Ratio $\frac{F}{\overline{F}}$
k_o	Luminosity coefficient, sec per km
k_1	Luminous efficiency
L	Luminosity, foot candle
M	Meteor magnitude
M_v	Meteor visual magnitude
m	Meteor mass, grams
m_o	Meteor mass at zero visual magnitude, grams
m_p	Mass of projectile, grams
N	Meteor flux, number per sq. meter day
N_M	Meteor flux at a given magnitude, number per sq. meter day

N_o	Meteor flux at zero visual magnitude, number per sq. meter day
N_p	Penetrating meteoroid flux, number per sq. meter day
N_t	Total meteoroid flux, number per sq. meter day
n	Velocity index; number of trials
P_r	Probability of rth event
p	Probability of single event in a single trial; penetration depth, cm
q	$(1 - p)$
R	True reliability
$\bar{R}$	Most probable reliability
t	Duration of meteor trail, secs
$\bar{t}$	Equivalent single sheet thickness, cm
t_f	Thickness of individual sheet, cm
V	Meteor velocity, km per sec
V_o	Meteor velocity at zero visual magnitude, km per sec
V_p	Relative impact velocity of projectile, km per sec
V_m	Relative impact velocity of meteoroid, km per sec
α	Meteoroid flux-mass constant, gm impacts per sq. meter day
β	Meteoroid flux-mass index
η	Earth shielding factor
ρ_m	Meteoroid density, gm per cm^3
ρ_p	Projectile density, gm per cm^3

ρ_t Target material density, gm per cm^3

τ Mission time in environment, days

2.0 METEOR THEORY

A precise definition of all the factors involved in the formulation of a design meteoroid environment is not currently available for the entire particle spectrum. While it is true that steps are being taken to obtain the data that has been lacking, the present generation of space-vehicles will be designed long before the results are available. Fortunately, it is possible to synthesize a model environment based on the known facts, using reasonable assumptions whenever necessary. An outline of the fundamentals involved in this task is presented in the ensuing text, without recourse to the history of meteor astronomy which may be obtained from references 1 and 2.

2.1 METEOR MAGNITUDE

The apparent magnitude of a star or a meteor is a measure of its luminosity as observed from the earth, relative to a reference stellar zero magnitude. A logarithmic comparative scale was adopted in 1850 based on the equivalence of a magnitude interval of unity to a luminosity ratio of 2.512. That is

$$\frac{L_1}{L_2} = 2.512\left(M_2 - M_1\right) \tag{2.1}$$

where M_1 and M_2 are the magnitudes and L_1 and L_2 the corresponding luminosities.

In logarithmic form, equation (2.1) is

$$\log_{10}\left(\frac{L_1}{L_2}\right) = 0.4\left(M_2 - M_1\right) \tag{2.2}$$

The scale is inverted in that increasing positive magnitudes are indicative of fainter objects.

A "visual" magnitude scale is most commonly used in meteor studies in spite of the fact that photography and radio astronomy have long since replaced the visual and optical observational methods. The more recent determinations of meteor flux were obtained in terms of photographic and radar magnitudes which were then converted into visual magnitudes by means of predetermined correlation constants.

Whichever scale is used, it functions as a means of classification of the meteoroid population in terms of flux, velocity, and, more recently, density.

A relationship between the absolute visual magnitude of a meteor, M_v, which is defined as the magnitude at a distance of 100 km in the direction of the zenith and the luminous flux, I, in visual ergs per second, has been derived by Öpik, reference 4.

This relationship is,

$$\log_{10} I = 9.72 - 0.4M_v \tag{2.3}$$

based on a stellar magnitude of -26.72 for the sun and the energy distribution of solar radiation.

2.2 THE RELATIONSHIP BETWEEN METEOR FLUX AND VISUAL MAGNITUDE

The number of meteors dN_M appearing in the atmosphere between visual magnitudes M_v and $M_v + dM_v$, is given by the incremental law,

$$dN_M = a.r^{M_v}.\ dM_v \tag{2.4}$$

where a is a constant and r is the ratio of the increase in the number of meteors between magnitudes M_v and $M_v + 1$.

Integrating equation (2.4) between the limits $M_v = -\infty$ and M gives the cumulative law. In logarithmic form, this is,

$$\begin{aligned} \log_{10} N_M &= M_v . \log_{10} r + \left\{ \log_{10} a - \log_{10}(\ln r) \right\} \\ &= M_v \cdot \log_{10} r + \log_{10} N_o \end{aligned} \tag{2.5}$$

where N_o is the number of meteors with $M_v = 0$ and brighter, and r is the same as in the incremental law.

The cumulative law is the basic concept in the definition of the meteoroid environment and there is no disagreement amongst astronomers as to its validity.

Values of r vary between 2.0 and 4.0, and of N_o, between 1.0×10^6 and 1.9×10^5, as a result of the different observational techniques used, the uncertainties in the observations, and in the correction factors involved.

McKinley, in reference 2, gives the flux-magnitude relationships favored by Watson, Millman, and Hawkins and Upton, as:

a. Watson (1956).- $\log_{10} N_M = 5.88 + 0.40\ M_v$ for $-3 \leq M_v \leq 10$

b. Millman.- $\log_{10} N_M = 6.0 + 0.57\ M_v$ for $-10 \leq M_v \leq 0$

$\log_{10} N_M = 6.0 + 0.50\ M_v$ for $0 \leq M_v \leq 3$

$\log_{10} N_M = 6.3 + 0.40\ M_v$ for $3 \leq M_v \leq 10$

c. Hawkins and Upton.- $\log_{10} N_M = 5.27 + 0.537\ M_v$ for $-1 \leq M_v \leq 10$

The limiting magnitude of +10 in all of these expressions is also the limit of the reliable radar observations to date and until systematic observations can be extended beyond this limit, it is necessary to assume that they are applicable up to $M_v = +15$.

One is forced to agree with Hawkins and Upton's contention that as $M_v \rightarrow \infty$, r must approach a value between 1 and 0, to avoid the inference that there is an infinite number of meteoroids in the universe.

A plot of N_M as a function of M_v, reproduced from reference 2, is presented in figure 1 to show the relative significance of the three relationships listed above on the Apollo spacecraft. The number of meteors of zero magnitude and brighter is based on the mean hourly flux rate of the sporadic meteor activity alone. This mean hourly rate is obtained from the results of several years of photographic observations, and for the Super-Schmidt camera collection area of 5,980 km^2 at an altitude of 90 km.

Meteor flux may be quoted as the number per square meter per hour or per day, or as the number over the entire surface area of the earth per day. In the latter case, the surface area of the earth is calculated at an altitude of 100 km.

2.3 THE CORRELATION OF METEOR MASS AND FLUX

Due to the evidence that most meteors break up upon entry into the earth's atmosphere, the most reliable method of calculating the mass of a meteor is by the relationship between the luminosity and the kinetic energy of a meteor,

$$I.t = \frac{1}{2} k_1 \cdot mV^2 \tag{2.6}$$

In this expression, I is the luminous flux which is related to the meteor magnitude M_v by equation (2.3), t is the time during which the meteor is visible, k_1 is the luminous efficiency factor, and $\frac{1}{2} mV^2$ is the kinetic energy of the meteor.

The value of M_v quoted is generally based on the photographic magnitude corresponding to the point of maximum luminous flux of the meteor trail. As a result, equation (2.6) may only be used for meteors which exhibit very little change in magnitude over the length of the trail.

Most meteors exhibit a variation in luminous flux along the length of the trail, and the time-histories of three types are shown in figure

In the general case, equation (2.6) must be replaced by,

$$\int_t^{\infty} I \cdot dt = \frac{k_1}{2} \cdot mV^2 \tag{2.7}$$

where the integration limits refer to the luminosity between the time when the mass is m and $+\infty$, when the meteoroid enters the atmosphere.

The terminal mass is generally zero for most photographic and radio meteors, hence it is possible to calculate the original mass of the meteoroid, m_∞, by integrating $I \cdot dt$ between the limits $+$ and $-\infty$, that is,

$$\int_{-\infty}^{+\infty} I \cdot dt = \frac{k_1}{2} \cdot m_\infty \cdot V^2 \tag{2.8}$$

Until very recently, it has not been possible to determine the luminous efficiency directly for various reasons. Most of the determinations of meteor mass have relied upon theoretical considerations of the laws of atomic physics, and estimates of k_1 have ranged between 2×10^2 and 2×10^4. Foremost in this field has been the work of Öpik, and in reference 4, he has published a table of values of $k_o = \frac{k_1}{V^n}$ for various meteor velocities ranging from 5 to 84 km/sec.

This quantity, k_o, is sometimes referred to as the luminosity coefficient.

The dependence of k_1 on meteor velocity to some power n is recognized amongst astronomers and it is thought that for the brighter photographic meteors, say up to magnitude +4.0, n is unity. A relationship for the fainter photographic and radio meteors remains to be established.

In the calculation of meteor mass, the astronomers actually use k_o rather than k_1 so that equation (2.8) is rewritten as,

$$\int_{-\infty}^{+\infty} I \cdot dt = \frac{k_o}{2} \cdot V^3 \cdot m_\infty \qquad (2.9)$$

A zero magnitude mass is established using the appropriate velocity, and then the mass value for increasing or decreasing positive magnitudes is obtained from the assumption of a mass ratio of 2.512 per unit magnitude step. It is also assumed that the mass of a meteor is directly proportional to its luminous flux so that increasing positive magnitudes correspond to decreasing masses.

The expression linking mass and magnitude is,

$$m = \frac{K}{10^{0.4M_v}} \qquad (2.10)$$

from which

$$\frac{m_1}{m_2} = 10^{0.4\left(M_{v=2} - M_{v=1}\right)} = 2.512^{\left(M_{v=1} - M_{v=2}\right)}$$

A summary of the zero magnitude mass, velocity assumed, luminosity coefficient used when known and meteoroid density is as follows:

Watson (1941) –	$m_o = 0.25$ gm	$V_o = 55$ km/sec
	$k_o = ?$	$\rho_m = 3.4$ gm/cc
Whipple (1952) –	$m_o = 1.25$ gm	$V_o = 40$ km/sec
	$k_o = 8.5 \times 10^{-5}$ sec/km	$\rho_m = 4$ gm/cc
Whipple (1957) –	$m_o = 25.0$ gm	$V_o = 28$ km/sec
	$k_o = 1.24 \times 10^{-5}$ sec/km	$\rho_m = 0.05$ gm/cc
Whipple & Hawkins – (1958)	$m_o = 0.15$ gm	$V_o = 30$ km/sec
	$k_o = 3.54 \times 10^{-5}$ sec/km	$\rho_m = ?$
McCrosky & Posen – (1961)	$m_o = 0.17$ gm	$V_o = 28.9$ km/sec
	$k_o = 8.5 \times 10^{-5}$ sec/km	$\rho_m = ?$
Öpik (1958) –	$m_o = 1.29$ gm	$V_o = 42$ km/sec
	$k_o = 1.06 \times 10^{-5}$ sec/km	$\rho_m = < 0.1$ gm/cc
Öpik (1958) –	$m_o = 0.29$ gm	$V_o = 42$ km/sec
	$k_o = 4.98 \times 10^{-5}$ sec/km	$\rho_m = 3.4$ gm/cc
0.1 Whipple (1961) –	$m_o = 2.5$ gm	$V_o = 28$ km/sec
	$k_o = 1.24 \times 10^{-4}$ sec/km	$\rho_m = 0.5$ gm/cc

McCrosky & Cook (1962) — $m_o = 2.0$ gm $\quad V_o = 28$ km/sec

$k_o = 2.29 \times 10^{-5}$ sec/km $\quad \rho_m = 0.6$ gm/cc

The immensity of the problem of assigning the zero magnitude mass is exposed by this historical resume of the varying estimates of the astronomers. The acquisition of data from the Trailblazer projects of 1962, when artificial meteors of known mass were fired into the atmosphere and photographically observed from ground stations, has resulted in a directly calculated value of $k_o = 2.29 \times 10^{-5}$ sec/km as determined by Cook, Jacchia, and McCrosky.

This value results in the zero magnitude mass calculated by McCrosky and Cook, ref. 6, shown in the last line of the above summary. It is interesting to note that the value of k_o obtained by Hawkins and Upton, using an ionization efficiency, the counterpart of luminous efficiency in radio astronomy, is no more than one order of magnitude less than the Cook, Jacchia, and McCrosky value mentioned previously.

The relationship between meteor mass and the particle flux is obtained from equations (2.5) and (2.10) and is of the form,

$$N = \alpha \cdot m^{\beta} \tag{2.11}$$

where α and β are constants, N is the impact rate and m is the meteoroid mass.

When N is measured in impact rate per square meter per second and m is in grams, the values of α and β are as follows:

	Source	α	β	Mass Range (gm)
a.	Meteors	3.715×10^{-13}	-1.35	10^{-3} to 10^{0}
b.	1957 Whipple	1.318×10^{-12}	-1.00	10^{-9} to 10^{0}
c.	1961 Whipple	5.012×10^{-13}	-1.186	10^{-9} to 10^{0}
d.	1956 Watson	5.129×10^{-15}	-1.00	10^{-9} to 10^{0}
e.	0.1 Whipple 1957	1.318×10^{-13}	-1.00	10^{-9} to 10^{0}
f.	0.1 Whipple 1961	5.012×10^{-14}	-1.186	10^{-9} to 10^{0}

The values for (a), (b), and (c) were obtained from reference 7, (d) is based on Watson's value of $m_o = .25$ gm, the flux-magnitude relationship

of section 2.2, and 90×10^6 meteors per day at $M_v = +5$. The zero magnitude mass of (b) and (c) is 25 gms, whereas (e) and (f), acting on Whipple's suggestion in reference 7, employ $\frac{1}{10}$ of this value.

Log-log plots of some of these flux-mass relationships are given in figure 3.

Figure 3 also indicates the change in slope which results if the satellite data of reference 8 is representative of the environment in the entire earth-moon system.

Whipple's contention of a concentration of dust around the earth which follows an approximately inverse 1.4 power law in distance from the earth's surface to about 10^5 km, reference 7, is shown in figures 4 and 5.

2.4 METEOR VELOCITY

One of the facets of the meteoroid environment that has received a great deal of attention from the astronomers is the problem of the limiting maximum velocity. Since the beginnings of the scientific obser vations the origin of meteors has been the subject of controversy. Basically, if meteors are members of the solar system, they must have closed orbits and the limiting heliocentric velocity at the earth's distance from the sun for this case is 42 km/sec.

As the earth's heliocentric velocity is approximately 30 km/sec, in the extreme case of a retrograde meteor in the plane of the ecliptic, the observed velocity relative to the earth cannot exceed 72 km/sec. Whipple in reference 6 gives a value of 73 km/sec including a slight additional effect due to the earth's gravitational potential.

Primarily as the result of radio velocity observations, astronomers are now in agreement that practically all the meteors which have been observed to date are members of the solar system. McKinley, in reference 2, states that of 11,000 radio meteors, only 32 had a velocity in the range of 75 to 79 km/sec and there were none exceeding 80 km/sec. He concludes that some of these could be explained by the 5 percent error in the reduction process.

Both Lovell, reference 1, and Jacchia and Whipple, reference 5, in their radio and photographic velocity determinations of several hundred meteor sightings could find no more than 1 percent that had velocities exceeding the critical value.

Thus it seems conclusive that the upper limit of the geocentric velocity is approximately 72 km/sec.

In the case of a direct meteor in the ecliptic, the observed velocity relative to the earth must, by the same token, be approximately 12 km/sec.

Within this range of 12 to 72 km/sec for the photographic and radio meteors, the average velocity has been calculated by various investigators. Thus Whipple, in reference 3, gives an average of 28 km/sec for photographic meteors. In reference 2, McKinley reports that the average observed velocity obtained for the 11,000 radio meteors is 44.7 km/sec, while the radio results for two sets of nearly 2,000 radio observations made at Jodrell Bank in England were 44.7 and 39.2 km/sec. For the photographic meteor observations, McKinley reports that the average entry velocity of 621 meteors reduced by Jacchia, Hawkins, and Southworth is 35.6 km/sec, and 34.3 km/sec for the 2,433 velocities determined by McCrosky.

The characteristic velocity distribution plots for radio and photographic meteors are shown in figures 6 and 7.

A program to determine the average entry velocity using McCrosky's data for the 2,433 photographic meteors, as well as the average per magnitude interval, has recently been concluded within the Spacecraft Technology Division, reference 10.

The preliminary results are shown in figure 8, the average in this case being 32.7 km/sec.

Velocity variation in terms of visual magnitude has received scant attention, and Whipple's attempt to establish a scale, reference 3, remains the only one published by the experts in this field.

The entry velocity at the edge of the earth's atmosphere cannot be less than 11 km/sec for a particle starting from rest within the solar system. Whipple, in reference 3, says that higher velocities can occur for nearly circular orbits by inclination of the orbital plane to that of the earth. For this reason, he arbitrarily chose a mean value of 15 km/sec for the smallest particles and then assumed a linear variation between this value and the average velocity for the photographic meteors.

Figure 9 is a plot of geocentric velocity as a function of visual magnitude for Whipple's estimate, together with the author's estimates based on the average velocities cited in this section.

2.5 THE DENSITY OF METEOROIDS

The examination of meteorites found on the earth, which are meteoroids that have survived the passage through the earth's atmosphere, has established the fact that:

a. Their chemical composition is unlike any rocks found on the earth.

b. About 90 percent are stony in character, with an average density of 3.5 gm/cc.

c. About 10 percent are iron-nickel with an average density of 7.8 gm/cc.

The identification of meteor orbits which do not exhibit any great degree of eccentricity and, in addition, have aphelion points inside the orbit of Jupiter, has led to the belief that meteorites originate in the asteroidal belt between Mars and Jupiter.

Meteorites are considered as part of the total meteor flux and are commonly called asteroidal meteors. The percentage of the total flux that is asteroidal varies between 10 percent, as determined by Jacchia and Whipple in reference 5, based on the orbital characteristics of meteors, and no more than 2 percent, based on the photographic evidence of fragmentation.

This latter figure is the opinion of both McCrosky and Cook of the Harvard Meteor Department, and it is considered applicable within the range of visual magnitudes 0 to +5.

Radio meteor studies to magnitude +10 currently indicate that fragmentation is again predominant so that by the same reasoning it seems likely that the asteroidal content is very small.

Considering the evidence of meteorites, and fireballs, it is a fair assumption that the asteroidal content of the total flux increases for magnitudes brighter than zero.

The density of the asteroidal component of the total flux, because of the preponderance of stony meteorites, is generally given as 3.5 gm/cc

Association of shower meteor orbits with comet orbits was first noticed in 1862, and since that time 12 meteor streams have been found to have nearly the same orbital characteristics as 9 comets. A further 20 streams have been tentatively identified as of cometary origin,

reference 5. In the same reference, Whipple states that the only proven source of meteors is cometary, and that when more comet orbits are known it may be possible to link them to other streams.

The sporadics or non-shower meteors are assumed to be dispersed particles from older comets which no longer travel in their original streams.

The cometary meteor model has been described by Whipple as an icy conglomerate and by Opik as a dust-ball. Both concepts envisage a loose aggregate of particles with an overall density of <1 gm/cc, with the individual particles having higher densities.

Whipple's value for the density of cometary meteors, associated with his 1957 estimate of $m_o = 25$ gm/cc was 0.05 gm/cc, reference 3. This value resulted in plausible luminous efficiencies of the order of 10^{-3} and was consistent with the frangible cometary model. He notes that assuming a density of stone, 3.5 gm/cc, led to the impossible conclusion that practically all of the kinetic energy of an ordinary meteor is transformed into light.

Other estimates of the density of cometary meteors obtained verbally from McCrosky, Cook, and Jacchia of Harvard, ranged between 0.3 gm/cc to 0.6 gm/cc.

It was agreed that the value of 0.5 gm/cc being used in the Apollo calculations was a good number.

In the opinion of Jacchia, the density of meteors associated with the Taurid shower is greater than that for the average cometary meteor. This is because the associated comet Encke is old enough to have lost its low density particles and the "core" particles are now predominant. He estimates the composition is rather like sandstone and that the density is approximately 1 gm/cc.

Assigning a single meteoroid density to the entire magnitude range does not seem plausible. Whipple, in reference 3, states that there is no evidence to justify the extrapolation of densities measured among visual meteors to the extremely faint ones. He says that the argument that the fragments from a large mass of low density could very well be of higher density is tenable.

Whipple's latest approach to the subject of density variation is given in reference 7 as the relationship,

$$\log_{10} \rho = 1.03 - .214 \log_{10} m \qquad (2.12)$$

where ρ is the meteoroid density in gm/cc and m is the meteor mass in grams. This relationship allows ρ to vary from a high value of 7.8 gm/cc for particles of a few microns diameter to very low densities for bright meteors.

The alternatives to this approach, adopted in this paper, are:

a. An all-cometary flux model with $\rho_m = 0.5$ gm/cc or,

b. A dual flux model in which 90 percent has a value of $\rho_m = 0.5$ gm/cc and 10 percent $\rho_m = 3.5$ gm/cc.

2.6 THE DISTRIBUTION OF METEOROID ORBITS

Until very recently, photographic and radio evidence showed that meteoroid orbits are concentrated in a narrow band within an inclination of 25° on either side of the ecliptic plane.

Recent evidence obtained from the 1962 Harvard Radio Meteor observations up to magnitude +10 confirms the presence of a "toroidal" belt of circular orbits suspected by earlier investigators. This belt is at 90° to the ecliptic. Up to magnitude +5, the concentration is as described in the first paragraph, while between +5 and +10 there is a mixture of both concentrations.

The majority of sporadic and shower meteors are in direct orbit around the sun, that is, they approach the earth from behind while the toroidal meteors are retrograde.

3.0 HIGH VELOCITY IMPACT ON METALLIC TARGETS

Penetration equations for particles impacting semi-infinite metallic targets are of the form:

$$\frac{p}{d} = K.X_1^{\alpha} \cdot X_2^{\beta} \cdot X_3^{\gamma} \cdot X_4^{\delta} \cdot X_5^{\epsilon}$$

where p is the penetration depth in the target, d is the characteristic dimension of the projectile, and X_1, X_2, X_3, X_4, et ceteras are physical and mechanical properties of the projectile and the target material in dimensionless form. K is a coefficient which compensates for the properties which have been neglected.

The most reliable experimental data obtained to date has been with the use of the accelerated piston light gas gun, which is capable of projecting $\frac{1}{16}$" and $\frac{1}{8}$" glass spheres up to 22,000 feet per second.

Various experiments have covered the velocity range from about 5,000 feet per second up to 22,000 feet per second using different combinations of projectile and target material properties.

The number of dependent variables involved in the penetration process identified so far has been limited by the necessity of varying no more than two or three dimensionless parameters in obtaining a curve of least fit to the experimental data points. The dimensionless coefficient, K, compensates for the parameters which have been neglected. A recent innovation in the search for a generalized penetration law has been the appearance of computer programs which can handle up to 27 dimensionless variables in a mathematical expression which will give a surface of best fit in a hyper-plane. The lack of reliable really high speed data points and the scarcity of information regarding the many physical and mechanical properties of the projectile and target materials required for the program will delay the appearance of a generalized penetration law for some time.

In the meantime, the pressing needs of the Apollo program has forced the adoption of an interim penetration equation.

At this point, it is necessary to say something about the current state of knowledge of penetration mechanics up to the limits of present day projection devices.

3.1 SEMI-INFINITE TARGETS

Figure 10 shows a plot of the ratio of penetration depth to the projectile diameter as a function of the ratio of the impacting velocity and the speed of sound in the target material, V_p/C_t, and the density ratio ρ_p/ρ_t for high-speed impact into semi-infinite targets, reference 14.

At low values of V_p/C_t, the penetration depth varies as the $\frac{4}{3}$ power of the velocity, the theoretical predictions being substantiated by several investigators. Beyond the upper limit of this region, the penetration depth varies as the $\frac{2}{3}$ power of velocity. There appears to be a transition region in between the two slopes in which the penetration depth can change with velocity in almost any fashion, depending on various physical and mechanical properties of the projectiles and targets.

The shape of the crater and the condition of the impacting projectile has been determined to be a function of the impact velocity and the ratio of the projectile density to the target density. At low speeds, the crater is deep and narrow, the projectile penetrating the target without deformation, as the dynamic impact pressure is lower than the strength of the particle. This is the region where the $V^{4/3}$ law applies.

With an increase in velocity, the impact pressure is high enough to cause the projectile to break up into a few large pieces. This marks the beginning of the transition region mentioned previously. With a further increase in velocity, still within the transition region, the impact pressure is high enough to cause an increase in the number of fragments and a decrease in their size. The cavity is not quite as deep or as narrow in this velocity range. The final stage is reached when the projectile and target, under very high pressures generated at impact, are in the fluid state and the crater shape is hemispherical. It is in this region that the penetration depth is proportional to $V^{2/3}$.

In addition to the hemispherical crater, the rear side of the target sometimes exhibits a phenomena known as "spallation." This is a circular fracture caused by the tensile stresses produced by the reflection of the shock wave from the rear face and is a feature of brittle materials.

Reliable experimental data relating to projectile impact velocities exceeding a V_p/C_t ratio of 1.4 on structural materials such as aluminum, titanium and steel, or an impact velocity of about 23,000 feet per second, is not presently available, hence it is necessary to assume that the $\frac{2}{3}$ power and the fluid impact phenomena are applicable at meteoroid velocitie It is interesting to note that tests conducted on lead targets show a continuation of the $\frac{2}{3}$ slope up to the limiting V_p/C_t value of 4, reference 14.

3.2 PENETRATION FORMULAS FOR SEMI-INFINITE TARGETS

The penetration equations currently in use in the evaluation of Apollo structural reliability are developments of:

(a) The Charters and Summers empirical formula, which is,

$$\frac{p}{d} = 2.28 \left(\frac{\rho_p}{\rho_t}\right)^{2/3} \left(\frac{V_p}{C_t}\right)^{2/3} \tag{3.1}$$

This is a modified form of the original Charters and Locke expression.

(b) The theoretical Bjork formulas:

$$p = 1.09 \cdot \left(m_p \cdot V_p\right)^{1/3} \quad \text{For an aluminum projectile and target} \qquad (3.2)$$

and

$$p = .606 \cdot \left(m_p \cdot V_p\right)^{1/3} \quad \text{For a steel projectile and target} \qquad (3.3)$$

The empirical Charters and Summers expression was chosen because it has been substantiated by several other investigators with some slight variation in the coefficient and exponents, reference 11, and also because it was determined by reliable tests conducted at the highest velocities achieved to date. It should be mentioned that the light gas gun capable of velocities up to 23,000 feet per second was developed at the Ames Research Center, and that Charters, Locke, and Summers conducted all their tests at that facility.

Bjork in his theoretical treatment of the hypervelocity impact process neglected:

(a) The elastic waves because the stresses and particle velocities carried by them will always be less than those caused by the shock wave.

(b) The projectile and target material strengths which are always greatly exceeded by the impact pressures.

(c) The viscosity of the target material.

(d) The conduction of heat during the period of crater formation.

In addition, he assumed a cylindrical projectile of L/D = 1, a semi-infinite solid target, and the same material for the projectile and target, reference 12.

The substantiating experimental evidence claimed by Bjork in the same reference can apply equally well to the $V_p^{2/3}$ law. Riney, in reference 13, commenting on Bjork's assumptions, reports that the dependence of the cratering process on the material strength has recently been demonstrated by tests carried out at the Carnegie Institute of Technology. He also suggests that there is evidence to show the importance of target viscosity on the impact phenomenon.

In the same reference, Riney rewrites Bjork's equations for aluminum and steel in terms of V_p/C_t thus:

$$\text{Al on Al} \quad \frac{p}{d} = 2.09 \left(\frac{V_p}{C_t}\right)^{1/3} \tag{3.4}$$

$$\text{Fe on Fe} \quad \frac{p}{d} = 1.69 \left(\frac{V_p}{C_t}\right)^{1/3} \tag{3.5}$$

in which the increased coefficient compensates for the change in form. Plots of p/d as a function of V_p/C_t, using experimental data for aluminum on aluminum and steel on steel up to an impact velocity of 16,700 feet per second show a very good match for the $\frac{2}{3}$ slope and a mismatch for Bjork's $\frac{1}{3}$ slope. These plots are reproduced in figures 11 and 12 with the addition of the Atkins and Partridge data points mentioned by Bjork in reference 12. It can be seen that even at these higher velocities, there is no conclusive evidence in support of the $\frac{1}{3}$ slope.

The newer projection techniques such as the shaped charge, exploding wire, the electrostatic accelerator, as well as the developed light-gas gun, will yield reliable test data at velocities above 35,000 feet per second, in the not too distant future. Until that time, it will not be possible to resolve the difference between the empirical and the theoretical approaches to the cratering process.

3.3 DOUBLE-SHEET THIN METALLIC TARGETS

The current extent of knowledge of the penetration resistance of thin metallic double-sheet targets subjected to high-speed impact is primarily due to the work done by Summers at the Ames Research Center.

Early tests showed that the rear sheet of a double-sheet target, depending on its separation distance from the front sheet, could either be penetrated, perforated, or just dented. This led to the adoption of the "ballistic limit" as a measure of the penetration resistance of a multi-wall target. The ballistic limit is defined as the impact velocity required to damage the rear sheet of a structure to the point where it will no longer hold a pressure differential of 1 atmosphere without leaks. Spallation from the rear surface of the rear sheet is obviously accounted for by this criterion.

Figure 13 is a plot of the ratio of the total sheet thickness to the projectile diameter as a function of the ballistic limit, reference 15. It is evident that there are three regions of different slopes as in the case of the semi-infinite slab, reference 14.

In the first region, the total thickness of sheet required to resist penetration is a function of the first power of the velocity. There is a transition region and finally a high speed region in which the particle and target sheet exhibit fluid flow and the total thickness of sheet is proportional to the $\frac{2}{3}$ power of the velocity.

In the low speed region up to about 10,000 feet per second, the projectile and the material punched out of the front sheet forms a tight cluster of relatively large fragments. The major damage to the rear sheet is confined to a small central region with an overall scattering of craters. At high speed impact, above 20,000 feet per second, both the projectile and the target material removed from the front sheet are shattered into a thin shell of fine fragments. The front of the shell is hemispherical and travels at a slightly lower velocity than the original impact velocity, and after it strikes the rear sheet the material splashes back to the rear of the front sheet, some of it passing out through the hole. In high speed impact on a double-wall structure with a sufficient distance between sheets, the hemispherical front of the spray spreads itself over a large area of the rear sheet. The damage is more or less evenly distributed, failure generally occurring in the form of small cracks that radiate out of the center of the area. This indicates that the failure mode is more a pressure rupture than a perforation.

As a matter of fact, the ballistic limit is not strongly affected by sheet spacing below an impact velocity of 10,000 feet per second. However, it becomes more effective in the transition region, and above 20,000 feet per second the effect of spacing is much greater, reference 15. The fragmentation spray developing a hemispherical front will obviously spread over a larger area of the rear sheet given a large enough separation distance, which, in turn, results in a lower tensile stress level.

Tests indicate that the optimum meteoroid resistant double-sheet structure, without a filling material between the sheets, is probably obtained by making the front or "bumper" sheet just thick enough to break up the projectile and making the rear sheet the remainder of the required total sheet thickness. It is also interesting to note, while on the subject of the "bumper" sheet, that for a given mass per unit area, tests indicate that the material is unimportant.

The effect of a "filler" material such as a low-density polyurethane, glass wool, or any light, porous, cellular material is to increase the

"ballistic limit" for the same sheet spacing and thickness. This is due to the retardation of the particle cluster formed by the shattered bumper and projectile, and tests show the most effective to be the low density polyurethane, reference 15.

On the other hand, a honeycomb core between the two sheets lowers the ballistic limit compared to a double-sheet structure having the same characteristics but no core, reference 16. The cells of this type of core prevent the hemispherical front from expanding and thus there is a channeling action and a consequent concentration of force on a small area of the rear sheet.

For the same ballistic limit, the sum of the sheet thicknesses in a double-sheet target is always less than the thickness of a single sheet target in the high speed impact region. As a result, it is possible to define a penetration resistance efficiency factor K as the ratio of the total sheet thickness in a double sheet configuration, Σt_f, to the equivalent single sheet thickness, $\bar{t}$, or

$$\Sigma t_f = K \cdot \bar{t} \tag{3.6}$$

The penetration resistance efficiency factors for various double-wall structural combinations of sheet spacing and filler, calculated mainly from unpublished test data supplied by Summers, is given in Table 1. As far as is known, this table has not been published previously. It is presented in this paper with the knowledge that the factors contained in it have the general concurrence of Summers.

3.4 APPLICABILITY OF PENETRATION EQUATIONS TO FINITE TARGETS

Tests on semi-infinite targets subjected to high-speed impact indicate that as the thickness of the target is reduced a point is reached when the target is penetrated by the combined effects of cratering and spallation. The thickness of the target when this happens is approximately 1.5 times the crater depth. Thus, in designing a single sheet to withstand penetration at a given impact velocity, the thickness of the sheet would have to be at least 50 percent more than the penetration depth calculated by using the formulas developed for the semi-infinitely thick targets. Hence, it is assumed that any formula derived for thick targets can be used for thin sheet provided it is modified to include the spallation factor.

Summer's equation, when modified for this target, is:

$$\frac{t}{d} = 3.42 \left(\frac{\rho_p}{\rho_t}\right)^{2/3} \cdot \left(\frac{V_p}{C_t}\right)^{2/3} \tag{3.7}$$

Bjork's equations, in the form given by equations (3.2) and (3.3), become:

$$\text{Al on Al:} \quad t = 1.64 \left(m_p V_p\right)^{1/3} \tag{3.8}$$

$$\text{Fe on Fe:} \quad t = 0.91 \left(m_p V_p\right)^{1/3} \tag{3.9}$$

Equations (3.8) and (3.9) may be approximated by a single equation, which is assumed applicable to all combinations of target and projectile materials. The generalized equation is:

$$t = 3.42 \cdot \rho_p^{1/3} \cdot \rho_t^{-1} \cdot \left(m_p V_p\right)^{1/3} \tag{3.10}$$

A further modification introduces the target material sonic velocity into the equation, which becomes:

$$t = 5.85\ \rho_p^{1/3} \cdot \rho_t^{-1} \cdot \left(m_p \cdot \frac{V_p}{C_t}\right)^{1/3} \tag{3.11}$$

This equation is valid for all materials in which the sonic velocity is 5 km/sec, or for which the Young's modulus to density ratio is 10^8. The materials falling in this category are the usual structural materials, aluminum, titanium, magnesium, and steel.

For beryllium, $\left(C_t = 12.6 \text{ km/sec and } \rho_t = 1.835 \text{ gm/cc}\right)$, the equation would be:

$$t = 7.95\ \rho_p^{1/3} \cdot \rho_t^{-1} \cdot \left(m_p \cdot \frac{V_p}{C_t}\right)^{1/3}$$

$$= 4.34\ \rho_p^{1/3} \cdot \left(m_p \cdot \frac{V_p}{C_t}\right)^{1/3} \tag{3.12}$$

3.5. THE PENETRATING METEOROID FLUX

Assuming a spherical meteoroid, Summer's penetration equation for finite sheet, equation (3.7), can be rewritten as:

$$\bar{t} = 4.24\ \rho_m^{1/3} \cdot m_p^{1/3} \cdot \left(\frac{V_m}{C_t \cdot \rho_t}\right)^{2/3} \tag{3.13}$$

where

$\bar{t}$ = The equivalent single sheet thickness of a structure just capable of holding 1 psi pressure differential, cm.

V_m = Meteoroid impact velocity, km/sec

C_t = Sonic velocity of structural material, km/sec

ρ_m = Density of meteoroid, gm/cc

ρ_t = Density of structural material, gm/cc

m_p = Penetrating meteoroid mass, gm.

From equation (3.13).

$$m_p = \frac{(\bar{t})^3}{76.24\ \rho_m \cdot \rho_t^{-2} \cdot \left(V_m/C_t\right)^2} \tag{3.14}$$

The general form of the meteoroid flux-mass relationship is given in equation (2.11) as,

$$N = \alpha \cdot m^{\beta}$$

α and β are constants, m is the meteoroid mass in grams, and N is the flux rate in gram impacts per unit area per day. Substituting m_p for m results in an expression for the penetrating flux rate,

$$N_p = \alpha \left[\frac{(\bar{t})^3}{76.24\ \rho_m \cdot \rho_t^{-2}\left(V_m/C_t\right)^2}\right]^{\beta} \tag{3.15}$$

A similar expression can be obtained by using the modified Bjork equation, (3.11), that is,

$$N_p = \alpha \left[\frac{(\bar{t})^3}{200 \cdot \rho_m \cdot \rho_t^{-3} \cdot \left(V_m/C_t\right)} \right]^{\beta} \qquad (3.16)$$

Thus, for every structural component exposed to the meteoroid environment, there is a penetrating flux-rate, N_p, which is the number of penetrating meteoroids per unit area and time of mass m_p and heavier.

Figure 14 is a plot of N_p as a function of $\bar{t}$ for an aluminum structure, combining Summers and Bjork's equations with the current Apollo meteoroid flux-mass expressions.

4.0 PROBABILITY OF PENETRATION

Having determined the penetrating meteoroid flux for a given equivalent skin thickness and material, the total meteoroid population can be considered as consisting of only two types — penetrating and nonpenetrating.

If a trial can have one of two mutually exclusive results, (penetration and nonpenetration) and if the probability p of a penetration is constant over a series of n independent trials, then the probability of obtaining r penetrations is,

$$P_r = \frac{n!}{r!\ (n-r)!} \cdot p^r \cdot q^{n-r} \qquad (4.1)$$

where $q = (1-p)$.

The probability distribution of r is called the Binomial distribution since the probabilities can be obtained by expanding $(q+p)^n$ by the Binomial formula.

In the case of a spacecraft in the meteoroid environment, a trial is considered an impact and the probability of a penetration in a single impact is:

$$p = \frac{N_p}{N_t} \qquad (4.2)$$

where N_t is the total meteoroid flux and N_p is the penetrating flux for the spacecraft.

The value of p is assumed constant during a mission, as the effect of removing the meteoroids that strike a space vehicle from the total flux is insignificant. As an example, say the flux-mass equation is $N_t \times m = 1 \times 10^{-9}$ gm impacts per square foot per day. Then for a 10,000 square foot sampling area, the number of impacts up to and including a mass of 10^{-12} grams is,

$$N_t = 1 \times 10^7 \text{ per day}$$

For a given equivalent skin thickness of a space vehicle, the number of penetrating meteoroids for the same sampling area is,

$$N_p = 10 \text{ per day}$$

Then at the first trial, $p = 1 \times 10^{-6}$

After 10^6 trials, all of which were removed from the environment, and assuming one was a penetration,

$$p = \frac{9}{9 \times 10^6} = 1 \times 10^{-6}$$

If the 10^6 trials had included 4 penetrating meteoroids, then,

$$p = \frac{6}{9 \times 10^6} = 6.67 \times 10^{-7}$$

N_p is always very much smaller than N_t, hence the assumption of a constant p is valid.

The "mean" or the "expected number of penetrations" of the probability distribution of r is the product of the number of trials, n, and the probability of a single penetration in a single trial or impact, p, that is,

Expected number of penetrations, $r_e = n \cdot p$. (4.3)

The number of impacts, $n = N_t \cdot A \cdot \tau \cdot \eta$ (4.4)

where N_t = total meteoroid flux, gram impacts per unit area per day.

A = vehicle surface area

τ = time in the environment in days

η = earth shielding factor, which varies between 0.5 and 1.0

The substitution of equations (4.2) and (4.4) in (4.3) results in,

$$r_e = n \cdot p = N_p \cdot A \cdot \tau \cdot \eta \tag{4.5}$$

When the probability of a single penetration in a single impact is a "rare event", (p is very small) and the number of impacts is very large, the use of the binomial probability distribution relation in its exact form becomes unwieldy. Poisson's approximation to the binomial distribution,

$$P_r = \frac{(np)^r}{r!} \cdot e^{-n \cdot p} \tag{4.6}$$

Substituting for n.p from equation (4.5) gives,

$$P_r = \frac{\left(N_p \cdot A \cdot \tau \cdot \eta\right)^r}{r!} \cdot e^{-N_p \cdot A \cdot \tau \cdot \eta} \tag{4.7}$$

where r is the number of penetrations.

The probability of no penetration is,

$$P_o = e^{-n \cdot p}$$

or

$$\log_{10} P_o = -0.434\ n.p = -0.434\ N_p . A . \tau . \eta \tag{4.8}$$

This equation can be used either as a means of designing to a given probability of zero penetration, or to evaluate the value of P_o for a given structure.

The probability that the number of penetrations will not exceed a number m is the summation of the probabilities of each occurrence

up to m, including zero, that is

$$P_{r \leq m} = P_o + P_1 + P_2 \ldots + P_{r=m} \tag{4.9}$$

or

$$P_{r \leq m} = e^{-N_p . A . \tau . \eta} \times \sum_{r=0}^{r=m} \frac{N_p . A . \tau . \eta}{r!} \tag{4.10}$$

The probabilities of exactly 0, 1, 2, 3, and 4 penetrations and of not exceeding 1, 2, 3, or 4 penetrations for n.p values ranging from 0 to 1 is given in table 2.

The binomial distribution, when presented in the graphic form, is represented by a histogram and not a continuous curve. Events are measured along the abscissa, probabilities along the ordinate, and the histogram is constructed so that each rectangle is of unit width and centered about r = 0, 1, 2, 3, and so on. It follows that the probability of each event r is also the area of the rectangle on r, hence the sum of the probabilities up to any value of r is the area of the histogram up to that ordinate. The histogram for an expected number or "mean" of 5 is shown in figure 15.

The total area of a probability histogram can never exceed unity because by definition the summation of all the admissible values of r, including zero, of the "probability function," equation (4.6), is,

$$\sum_{r=0}^{r=s} e^{-np} = \frac{(np)^r}{r!} = 1 \tag{4.11}$$

5.0 RELIABILITY AND CONFIDENCE LEVEL

Although the probability of no penetration is generally used as the criterion for the structural integrity of a space vehicle exposed to the meteoroid environment, it is not a measure of reliability. The reliability of a component is usually determined from a statistical sample of identical tests, which is obviously not a practical proposition in the case of a space vehicle.

A method of calculating the reliability, together with an associated confidence level based on the expected number of penetrations over a very large number of identical missions, will be described in this section.

For a situation where $n.p$ is the most probable number of penetrations, it follows that,

$$n.p = \text{the most probable or average failure rate}$$

$$= \overline{F}$$

From this the most probable reliability is,

$$\overline{R} = 1 - \overline{F} \tag{5.1}$$

It is evident from figure 15 that in dealing with the most probable number there is a good probability of exceeding it. Thus the failure rate may be equal or greater than $\overline{F}$ approximately 50 percent of the time, and the actual reliability may be equal or less than $\overline{R}$ approximately 50 percent of the time. The confidence level, C, in the reliability being $\overline{R}$ or more is therefore about 50 percent.

In order to achieve a reliability R with an associated high confidence level the system must have a most probable failure rate less than $(1-R)$, that is

$$\overline{F} < F = (1-R) \tag{5.2}$$

The relationship between $\overline{F}$ and F may be illustrated by the two probability distributions shown in figure 16, which differ only in the number of trials (mission time).

To attain a failure rate in which one has 97.5 percent confidence, the average failure rate is approximately $\frac{1}{2}$ F when $np = 5$ and $\frac{2}{3}$ F when $np = 15$.

This ratio will be called k. Thus,

$$F = k.\overline{F}$$

$$= k.(np)$$

and

$$R = 1 - F$$

$$= \left[1 - k.(np)\right] \tag{5.3}$$

Values of k for various confidence levels are plotted in figure 17 as a function of $(a.np)$, where "a" is a large number of missions such that $(a.np) \gg 1$.

It may be seen that for $C = 0.5$, $k \rightarrow 1.0$ as may be expected. Also, for,

$$C = 0.90 \qquad k \rightarrow 1.3$$

$$= 0.95 \qquad k \rightarrow 1.4$$

$$= 0.975 \qquad k \rightarrow 1.5$$

For reliability purposes, the generally accepted confidence level $C = 0.975$ will be adopted, in which case $k = 1.5$.

Thus,

$$R = \left[1 - 1.5(n.p)\right] \tag{5.4}$$

when $C = 0.975$.

This means that, in order to quote a reliability in which one has a high confidence level, this reliability must be based on a failure rate which is 1.5 times the average failure rate. Conversely, the average failure rate must be $\frac{2}{3}$ of the guaranteed failure rate.

6.0 RELIABILITY - EQUIVALENT SKIN THICKNESS RELATIONSHIPS

The principles involving the evaluation of the shielding requirements for a vehicle in the meteoroid environment have now been established. All that remains is to directly relate reliability to the equivalent skin thickness in terms of flux parameters, penetration equation, and the number of failures.

Substituting equation (4.5) into equations (3.15) and (3.16) gives:

(a) Using Summers equation,

$$np = \alpha . A . \tau . \eta \left[\frac{(\bar{t})^3 . \rho_t^2 . C_t^2}{76.24\, \rho_m . V_m^2}\right]^{\beta} \tag{6.1}$$

(b) Using Bjork's equation,

$$np = \alpha . A . \tau . \eta \left[\frac{(\bar{t})^3 . \rho_t^{\,3} . C_t}{200 \; \rho_m \; . \; V_m} \right]^{\beta} \tag{6.2}$$

Thus, by equation (5.1)

$$R = \left\{ 1 - k . \alpha . A . \tau . \eta \left[\frac{(\bar{t})^3 . \rho_t^{\,2} . C_t^{\,2}}{76.24 \; \rho_m . V_m^{\,2}} \right]^{\beta} \right\} \tag{6.3}$$

using Summers' equation

and

$$R = \left\{ 1 - k . \alpha . A . \tau . \eta \left[\frac{(\bar{t})^3 . \rho_t^{\,3} . C_t}{200 \; \rho_m \; . \; V_m} \right]^{\beta} \right\} \tag{6.4}$$

using Bjork's equation

The penetration equations considered are examples of the most generally accepted empirical and theoretical expressions of the cratering phenomenon. Other forms of penetration equations are equally amenable to the procedure established in this paper for the ultimate relationship of equivalent thickness, $\bar{t}$ to the protective reliability, R.

A.1 MSC DESIGN ENVIRONMENTS

The design environment currently in use within MSC divides the total flux into two components in the following manner:

a. Asteroidal: Flux = 10 percent of the total

m_o = 1 gram

ρ_m = 3.5 gm/cc

β = -1.00

α = 4.5×10^{-10} gm impacts/meter^{2}day

V_m = 30 km/sec, or as in figure 9

Thus, by equation (2.11),

$$N.m = 4.5 \times 10^{-10} \text{ gm impacts/meter}^2\text{day}$$

Or in engineering units

$$N.m = 4.2 \times 10^{-11} \text{ gm impacts/feet}^2\text{day}$$

b. Cometary: Flux = 90 percent of the total

$$m_o = 2.0 \text{ gram}$$

$$\rho_m = 0.5 \text{ gm/cc}$$

$$\beta = -1$$

$$\alpha = 8.2 \times 10^{-9} \text{ gm impacts/meter}^2\text{day}$$

$$V_m = 30 \text{ km/sec, or as in figure 9.}$$

and

$$N.m = 8.2 \times 10^{-9} \text{ gm impacts/meter}^2\text{day}$$

$$= 7.66 \times 10^{-10} \text{ gm impacts/ft}^2\text{day}$$

The design environment is equivalent to a modified form of Whipple's 1957 flux-mass relationship, in which the value of $m_o = 2.5$ grams, as suggested in reference 7, and a meteoroid density of 0.5 gm/cc is used instead of 0.05 gm/cc. Thus the modified 1957 Whipple flux mass relationship is:

c.

$$N.m = 1.134 \times 10^{-8} \text{ gm impacts/meter}^2\text{day}$$

$$= 1.06 \times 10^{-9} \text{ gm impacts/ft}^2\text{day}$$

and

$$V_m = 30 \text{ km/sec, or as shown in figure 9.}$$

The equivalence of (c) to (a) + (b) can be demonstrated as follows:

From equation (3.15), with $\beta = -1$

$$N_p = \alpha \cdot \left[\frac{76.24 \cdot \rho_m \cdot V_m^2}{(\bar{t})^3 \cdot \rho_t^2 \cdot C_t^2}\right], \text{ where } \bar{t} \text{ is in cms.}$$

Substituting for $V_m = 30$ km/sec, $C_t = 5$ km/sec and $\rho_t = 2.78$ gm/cc,

$$N_p = \frac{354.24\ \alpha . \rho_m}{(\bar{t})^3} \qquad (1)$$

For (c), substituting for $\alpha = 1.134 \times 10^{-8}$, $\bar{t} = 10^{-1}$ cm, and

$$\rho_m = 0.5 \text{ gm/cc}$$

$$N_p = 2.01 \times 10^{-3} \text{ penetrations/ft}^2\text{day}$$

Also, for (a) + (b), again using $\bar{t} = 10^{-1}$ cm, and the appropriate values of α and ρ_m,

$$N_p = 3.54 \times 10^5\ (4.5 \times 10^{-10} \times 3.4 + 8.2 \times 10^{-9} \times 0.5)$$
$$= 1.99 \times 10^{-3} \text{ penetrations/ft}^2\text{day}$$

Hence, in terms of penetrating flux, and also np, the dual flux may be replaced by the 100 percent cometary model, (c).

A.2 CALCULATION OF P_o AND RELIABILITY, R

The basic data for a space-vehicle component on a lunar mission is as follows:

Surface area, $A = 520$ ft^2

Days in meteoroid environment; $\tau = 14$

Construction: An aluminum, double-wall without a filler, with equal sheet thicknesses of .017 in., 1.0 in. apart.

Design environment: $N.m = 1.06 \times 10^{-9}$ gm impacts/ft^{2}day

$$\rho_m = 0.5 \text{ gm/cc}$$

$$V_m = 30 \text{ km/sec}$$

From equation (3.6),

$$\text{equivalent thickness, } \bar{t} = \frac{\Sigma t_f}{K}$$

Using table I, K = 0.37 for a 1.0 in. double wall, no core

$$\therefore \bar{t} = \frac{.034}{.37}$$

$$= 0.092 \text{ in.}$$

On substituting in equation (6.1), for $\alpha = 1.06 \times 10^{-9}$, $\beta = -1$, $\rho_m = 0.5$ gm/cc, $\rho_t = 2.78$ gm/cc, $V_m = 30$ Km/sec, and $C_t = 5$ Km/sec, and using an earth shielding factor of 1.0, the

$$\text{expected number } np = 1.88 \times 10^{-7} \times \frac{A.\tau}{(\bar{t})^3}, \text{ where } \bar{t} \text{ is in cms} \qquad (2)$$

Converting to inches,

$$np = 1.147 \times 10^{-8} \times \frac{A.\tau}{(\bar{t})^3} \qquad (3)$$

Using equation (6.2), a similar expression for the expected number is obtained, that is,

$$np = 2.96 \times 10^{-8} \times \frac{A.\tau}{(\bar{t})^3}, \text{ for t in cms.}$$

and

$$np = 1.81 \times 10^{-9} \times \frac{A.\tau}{(\bar{t})^3}, \text{ for t in inches} \qquad (4)$$

Figures 18 and 19 are plots of np as a function of $\bar{t}$ for various values of the area-time product $A.\tau$ for both Summers' and Bjork's penetration theories.

Hence, when $\bar{t} = .092$ in. and $A.\tau = 7{,}290$ ft^{2}days,

a. Summers: np = .107

b. Bjork: np = .017

The probability of no penetration P_o is obtained from the curve given in figures 21 and 22.

Thus for the Summers' case,

$$P_o = 0.899$$

and for Bjork's, $P_o = 0.983$

The corresponding reliabilities and confidence levels obtained as described in section 5 are as follows:

		np	P_o	C	R
(a)	Summers	.107	.899	50.0%	.893
				97.5%	.839
(b)	Bjork	.017	.983	50.0%	.983
				97.5%	.975

If the void between the sheets were filled with a honey-comb core,

$$K = 1.00$$

and

$$\bar{t} = 0.034 \text{ in.}$$

		np	P_o	C	R
(a)	Summers	2.12	.120	50.5%	0
				97.5%	0
(b)	Bjork	.334	.716	50.5%	.666
				97.5%	.499

A.3 DESIGNING TO A GIVEN P_o OR R

A.3.1. Based on $P_o = 0.99$ –

From equation (4.8), $\log_{10} P_o^2 = -.434 \text{ np}$

$$\therefore \text{np} = \frac{-.0044}{-.434} = 0.0101$$

The equivalent single sheet thickness in aluminum is obtained from figure 18, using the Summers curve, and $A.\tau = 7{,}290\ ft^2$ days.

Thus, $\bar{t} = 0.202$ in.

Using table 1, and $\Sigma t_f = K.\bar{t}$, and considering a 2.0" double-sheet construction without a core,

$$\Sigma t_f = .23 \times .202$$
$$= 0.0465 \text{ in.}$$

The sheets could be equally divided into two 0.024 in., or the front or bumper sheet may be made only as thick as the diameter of the penetrating meteoroid, and the rest of the material added to the rear sheet.

In order to calculate the diameter, it is necessary to obtain the penetrating mass from equation (3.14), in inches.

$$m_p = \frac{(\bar{t})^3 \cdot \rho_t^2}{4.65\ \rho_m \cdot (V_m/C_t)^2}$$

The diameter is calculated by assuming a spherical meteoroid and the use of the appropriate density.

For this structure, $R = 0.99$ for $C = 50\%$

and $R = 0.985$ for $C = 97.5\%$

<u>A.3.2. Based on $R = \geq 0.99$ and $C = 97.5\%$.</u> –

From equation (5,5) $\bar{R} = \left[1 - k(n.p)\right]$

when $C = 97.5\%, \quad k = 1.5$

$$\therefore 0.99 = \left[1 - 1.5\ n.p\right]$$

and $n.p = 0.0067$

As before, the value of $\bar{t}$ can be obtained from figure 17, using the same criteria.

$$\therefore \bar{t} = 0.232 \text{ in.}$$

and

$$\Sigma t_f = .23 \times .232$$

$$= .053 \text{ in.}$$

Designing to a confidence level of 0.975 and a reliability of 0.99 results in a 14 percent increase in weight.

However, the increased confidence level in the reliability of the structure is sufficient compensation.

The question of material selection is covered in section B2. Sheet thickness and weight ratios relative to aluminum are given therein for the other commonly used materials.

As an example, the percentage increase in weight due to the increased confidence level can be offset by using magnesium instead of aluminum, providing its use is permissible.

A plot of np as a function of reliability for confidence levels of 97.5%, 95%, and 90% is shown in figure 20.

A.3.3. Designing to a controlled number of penetrations –

Sometimes it becomes necessary, due to weight limitations, to permit no more than a given number of penetrations within a specified time period. The procedure to be followed in this case is identical to that outlined in the previous sub-section, A3.1.

Figure 23 is a plot of np as a function of the number of events that should not be exceeded, for probabilities of 0.99, 0.995, and 0.999. Thus, if a certain design calls for a 0.99 probability of not exceeding two penetrations in 100 days, then from the curves,

$$np = 0.45$$

Using the Summers' criterion, equation (2),

$$(\bar{t})^3 = \frac{1.147 \times 10^{-8} \times A_{\tau}}{np}, \text{ where } \tau = 100 \text{ days.}$$

In this case, the concept of "reliability" is no longer valid. A structure that is designed to be penetrated is not "reliable" in the sense previously outlined for no penetration.

There is no need to specify anything other than the confidence that the probability of not exceeding n penetration in t days is 0.99 or 0.999.

The confidence is obtained from the lower curve of figures 21 and 22 which, for the example being considered, is 0.537.

Design charts for the direct determination of $\bar{t}$ for $P_{r \leq n} = 0.99$ and Summers' penetration equation are given in figures 24 and 25.

In one case the number of penetrations is limited for the total mission time τ and in the other for various lesser time periods.

As an example, a space-vehicle of 16,000 ft^2 is expected to remain in the environment for 500 days.

Then total $A\tau = 8 \times 10^6$ ft^2 days

Based on the philosophy of no more than one penetration every 30 days, $\bar{t}$ from figure 25 is 0.345 in.

If an average of no more than one penetration in 30 days were based on an actual six in 180 days, then $\bar{t} = 0.24$ in.

Should the average of one in 30 be based on an actual 17 throughout the total mission time of 500 days, then $\bar{t}$ is 0.175 in. approximately

Obviously, the actual design is based on the requirements of the vehicle or component to be protected.

A thickness of 0.342 in. insures that there will be no more than one in 30 days, whereas the value of $\bar{t} = 0.175$ in. being based on the average does not preclude the possibility that all 17 penetrations will occur in the last 30 days of the mission. The latter condition, being much more hazardous to both crew and vital system components, could not be tolerated.

B.1 MATERIAL COMPARISON

B.1.1 Sonic Velocity in Structural Materials –

$$C_t = \left(\frac{E_t \cdot g}{12 \cdot \rho_t}\right)^{1/2}$$

where

E = Young's Modulus, lb/in^2

ρ_t = Density, lb/in^3

g = 386.4 in/sec^2

Material	ρ_t	$E_t \times 10^{-6}$	C_t (ft/sec)	C_t (km/sec)
Magnesium	0.065	6.5	16,350	5
Aluminum	0.1	10	16,350	5
Titanium	0.16	16	16,350	5
Steel	0.30	30	16,350	5
Fiberglass	0.063	3	11,300	3.46
Plexiglass	0.043	0.45	5,170	1.58

B.2 SINGLE THICKNESS AND WEIGHT RELATIVE TO ALUMINUM

B.2.1 Summers' Equation –

From equation (3.13), converted to inches,

$$t = 1.67\ \rho_m^{1/3} \cdot m_p^{1/3} \cdot \left(\frac{V_m}{C_t \cdot \rho_t}\right)^{2/3}, \text{ cms}$$

or

$$t = K \cdot \left(C_t \cdot \rho_t\right)^{-2/3} \qquad (5)$$

Material	t (in)	t/t_{Al}	ρ_t (lb/in^3)	w (lb/in^2)	w/w_{Al}
Mg	9.6×10^{-3} K	1.33	0.065	6.25×10^{-4} K	0.87
Al	7.2×10^{-3} K	1.00	0.100	7.20×10^{-4} K	1.00
Ti	5.28×10^{-3} K	0.73	0.160	8.45×10^{-4} K	1.17
St	3.55×10^{-3} K	0.49	0.300	10.65×10^{-4} K	1.43
F.G.	12.5×10^{-3} K	1.73	0.063	7.87×10^{-4} K	1.09
P.G.	27.1×10^{-3} K	3.76	0.043	11.65×10^{-4} K	1.62

B.2.2 Bjork's Equation -

From equation (3.11), in inches

$$t = 2.30\ K.\rho_t^{-1}.C_t^{-1/3} \qquad (6)$$

for Al, Mg, St, and Ti

Material	t (in)	t/t_{Al}	ρ_t (lb/in^3)	w (lb/in^2)	w/w_{Al}
Mg	13.94×10^{-1} K	1.54	0.065	9.07×10^{-2} K	1.00
Al	9.06×10^{-1} K	1.00	0.100	9.06×10^{-2} K	1.00
Ti	5.66×10^{-1} K	0.625	0.160	9.06×10^{-2} K	1.00
St	3.02×10^{-1} K	0.333	0.300	9.06×10^{-2} K	1.00

REFERENCES

1. Lovell, A. C. B.: "Meteor Astronomy," Oxford University Press, New York, 1954.

2. McKinley, D. R.: "Meteor Science and Engineering," McGraw-Hill, New York, 1961.

3. Whipple, F. L.: "The Meteoritic Risk to Space-Vehicles," Vistas in Astronautics, Pergammon Press, Los Angeles, 1958.

4. Öpik, E. J.: "Physics of Meteor Flight in the Atmosphere," Interscience Publishers, Inc., New York, 1958.

5. Jacchia, L. G., and Whipple, F. L.: "Precision Orbits of 413 Photographic Meteors," Smithsonian Contributions to Astrophysics, Vol. 4, No. 4, Smithsonian Institution, Washington, D. C.

6. Whipple, F. L.: "Meteoritic Phenomena and Meteorites." Ed. C. S. White, and O. O. Benson.: "Physics of the Upper Atmosphere." University of New Mexico Press, Albuquerque, 1952.

7. Whipple, F. L.: "Particulate Contents of Space," Medical and Biological Aspects of the Energies of Space, Columbia University Press, 1961.

8. Alexander, W. M., McCracken, C. W., Secretan, L., and Berg, O. E.: "Review of Direct Measurements of Interplanetary Dust from Satellites and Probes," Report X-613-62-25, Goddard Space Flight Center, Greenbelt, Md.

9. Private communication from Dr. A. F. Cook, Smithsonian Institution, Astrophysical Observatory.

10. Unpublished Working Paper.

11. Maiden, C. J., Tardif, H. P., and Charest, J.: "An Investigation of Spalling and Crater Formation by Hypervelocity Projectiles," CARDE Tech. Memo AB.62, May 1960, Valcartier, Quebec, Canada.

12. Bjork, R. L.: "Effects of a Meteoroid Impact on Steel and Aluminum in Space," Report P-1662, December 16, 1958, the Rand Corporation.

13. Riney, T. D.: "Theory of High Speed Impact," (Summary Report, 3rd Nov. 1961), Technical Documentary Report No. APGC-TDR-62-20, March 1962, Air Force Systems Command, Eglin AFB, Florida.

14. Summers, J. L.: "Investigation of High-Speed Impact: Regions of Impact and Impact at Oblique Angles." TN-D94, October 1959.

15. Nyesmith, Robert, and Summers, J. L.: "An Experimental Investigation of the Impact Resistance of Double-sheet Structures at Velocities to 24,000 feet per second," TN-D1431, 1962.

16. Summers, J. L., and Nyesmith, C. Robert: "Evaluation of the Meteoroid Hazard," unpublished report, 1962.

$$\sum t_f = K.\bar{t}$$

	h	K
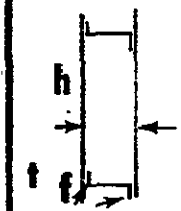 NO CORE	1.0 1.5 2.0	0.37 0.28 0.23
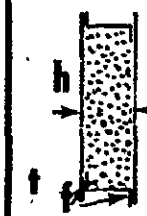 LOW DENSITY POROUS PLASTIC CORE	1.0 1.5 2.0	0.23 0.18 0.15
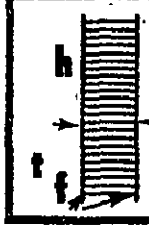 HONEYCOMB CORE	1.0 1.5 2.0	1.00 0.70 0.40

TABLE I.- PENETRATION EFFICIENCY FACTORS FOR DOUBLE-SHEET STRUCTURAL CONFIGURATIONS.

r	0	1	2	3	4	$\bar{<}1$	$\bar{<}2$	$\bar{<}3$	$\bar{<}4$
n.p	P_0	P_1	P_2	P_3	P_4	$P_0 + P_1$	$P_0 + P_1 + P_2$	$P_0 + P_1 + P_2 + P_3$	$P_0 + P_1 + P_2 + P_3 + P_4$
0	1.0	-	-	-	-	-	-	-	-
.01	.99005	.00990	.00005	-	-	.99995	1.00000	1.00000	1.00000
.10	.90484	.09048	.00452	.00015	.00004	.99532	.99984	.99999	1.00000
.20	.81873	.16375	.01638	.00109	.00006	.98248	.99886	.99995	1.00000
.50	.60653	.30327	.07582	.01264	.00158	.90980	.98562	.99826	.99984
.80	.44933	.35946	.14379	.03834	.00767	.80879	.95258	.99092	.99859
1.00	.36788	.36788	.18394	.06131	.01533	.73576	.91970	.98101	.99634
1.10	.33287	.36616	.20139	.07384	.02031	.69903	.90042	.97426	.99457

TABLE II.- PROBABILITIES OF EXACTLY AND NOT EXCEEDING r EVENTS.

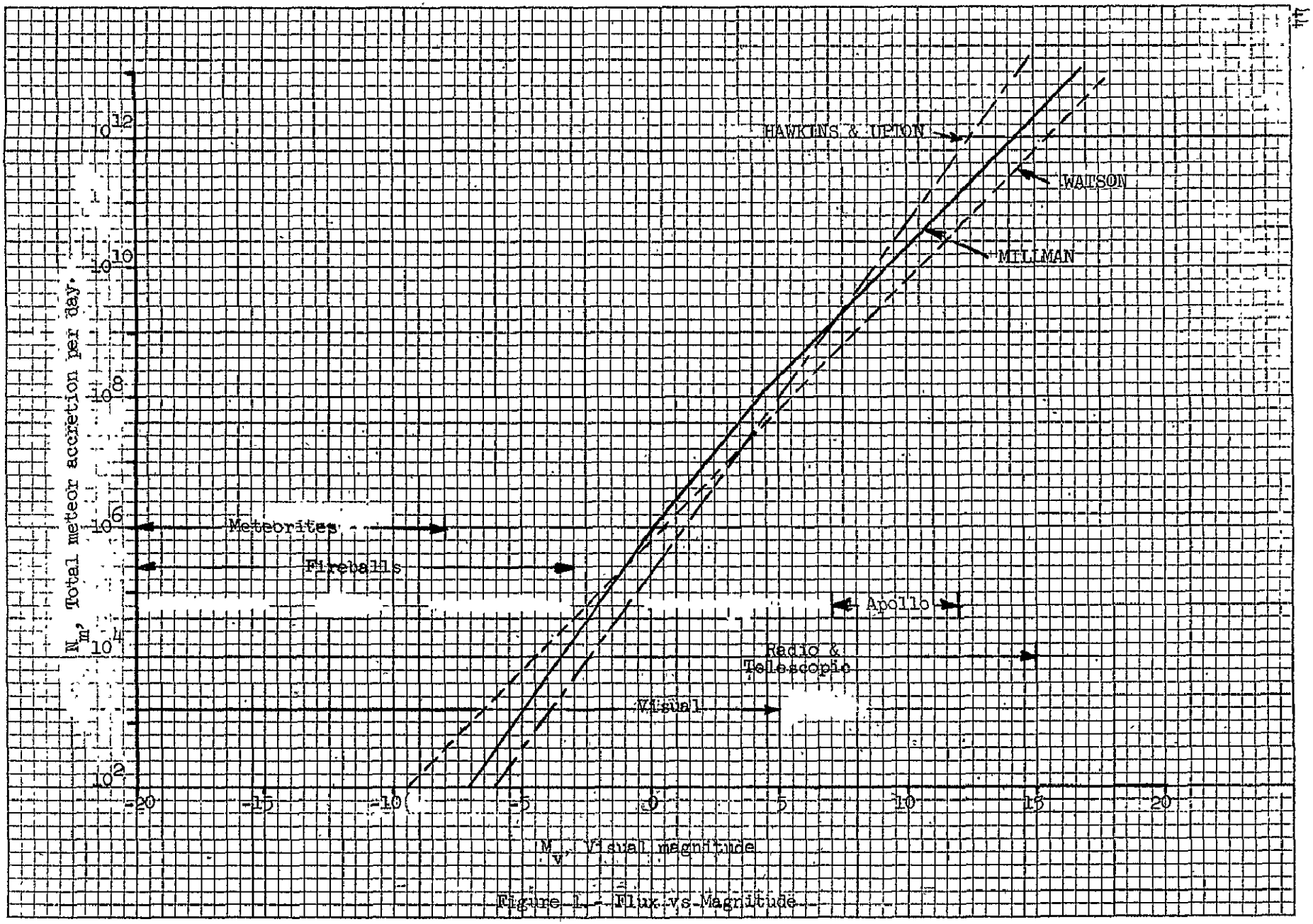

Figure 1. - Flux vs Magnitude

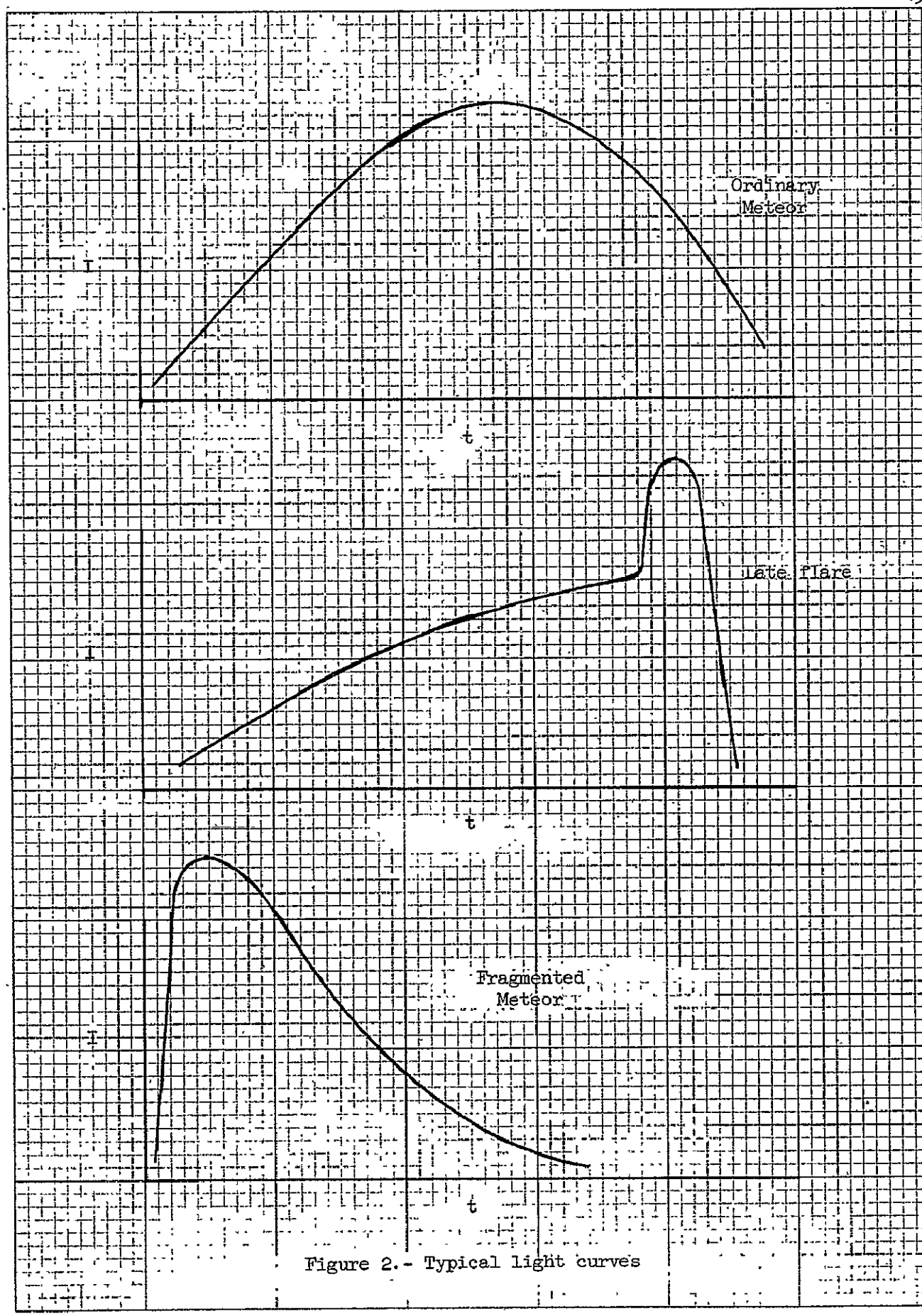

Figure 2.- Typical light curves

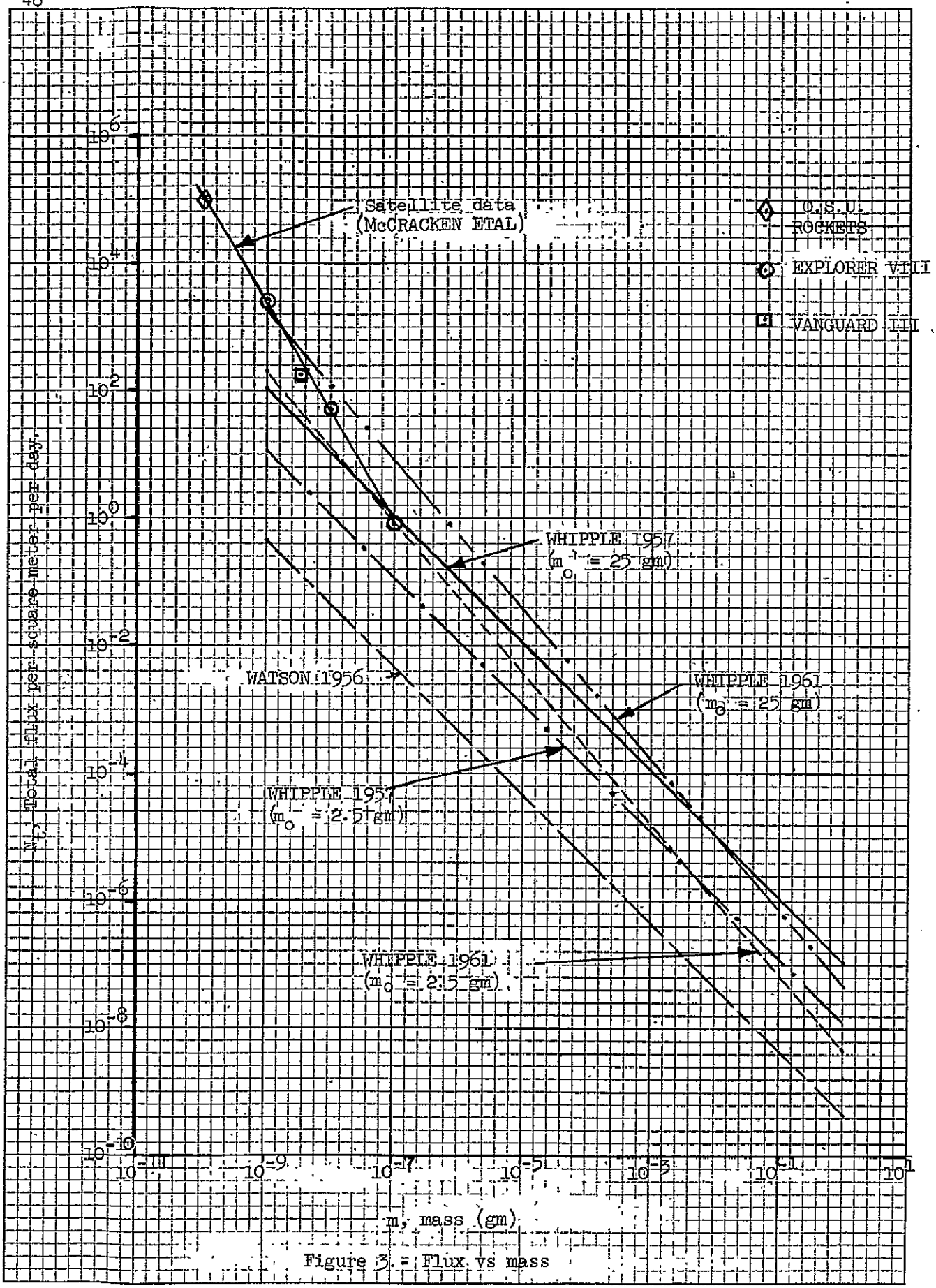

Figure 3. - Flux vs mass

Figure 4. - Height vs meteor mass.

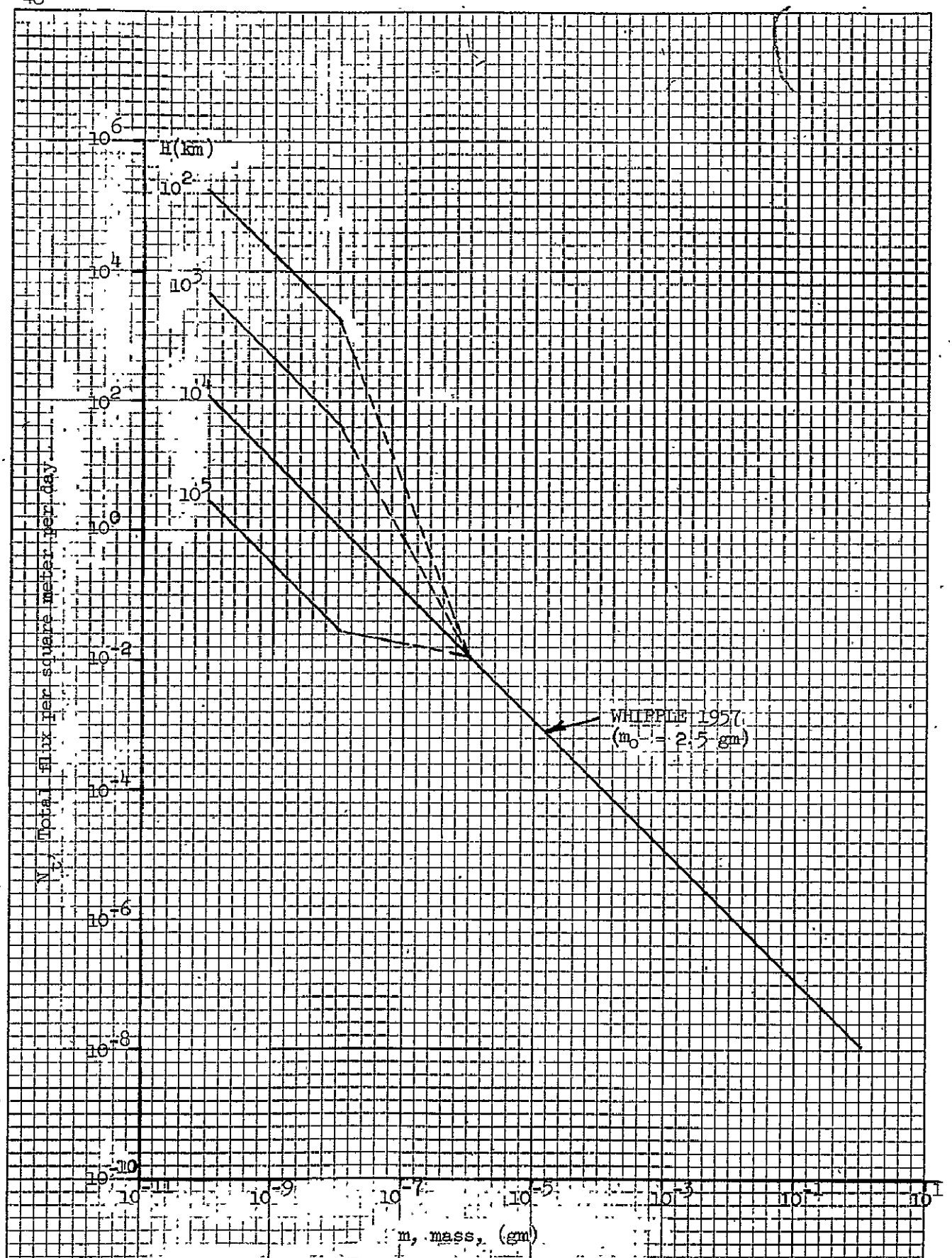

Figure 5.- Flux-mass variation with altitude-based on dust-belt concept.

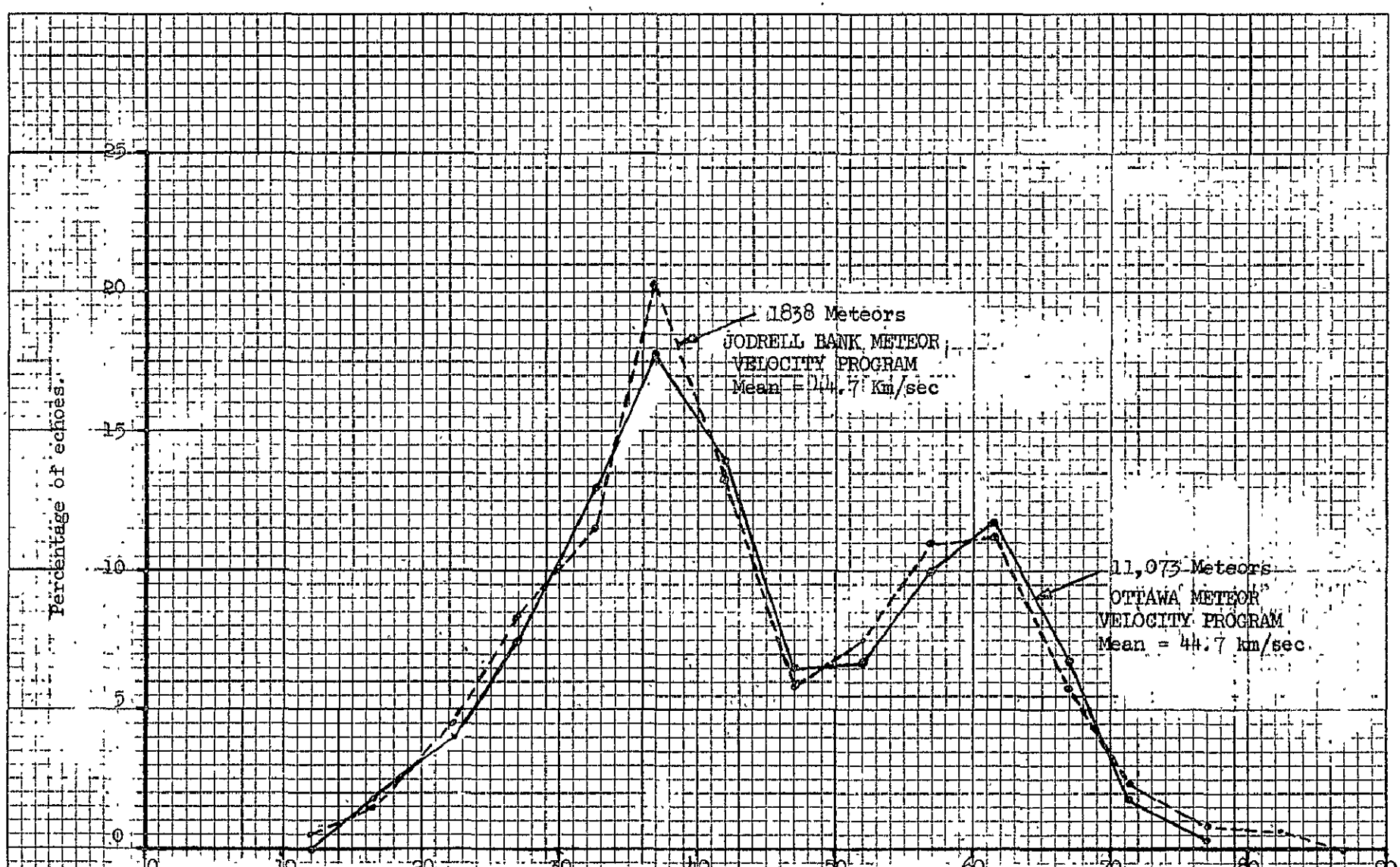

Figure 6. Normalized radio meteor velocity distributions.

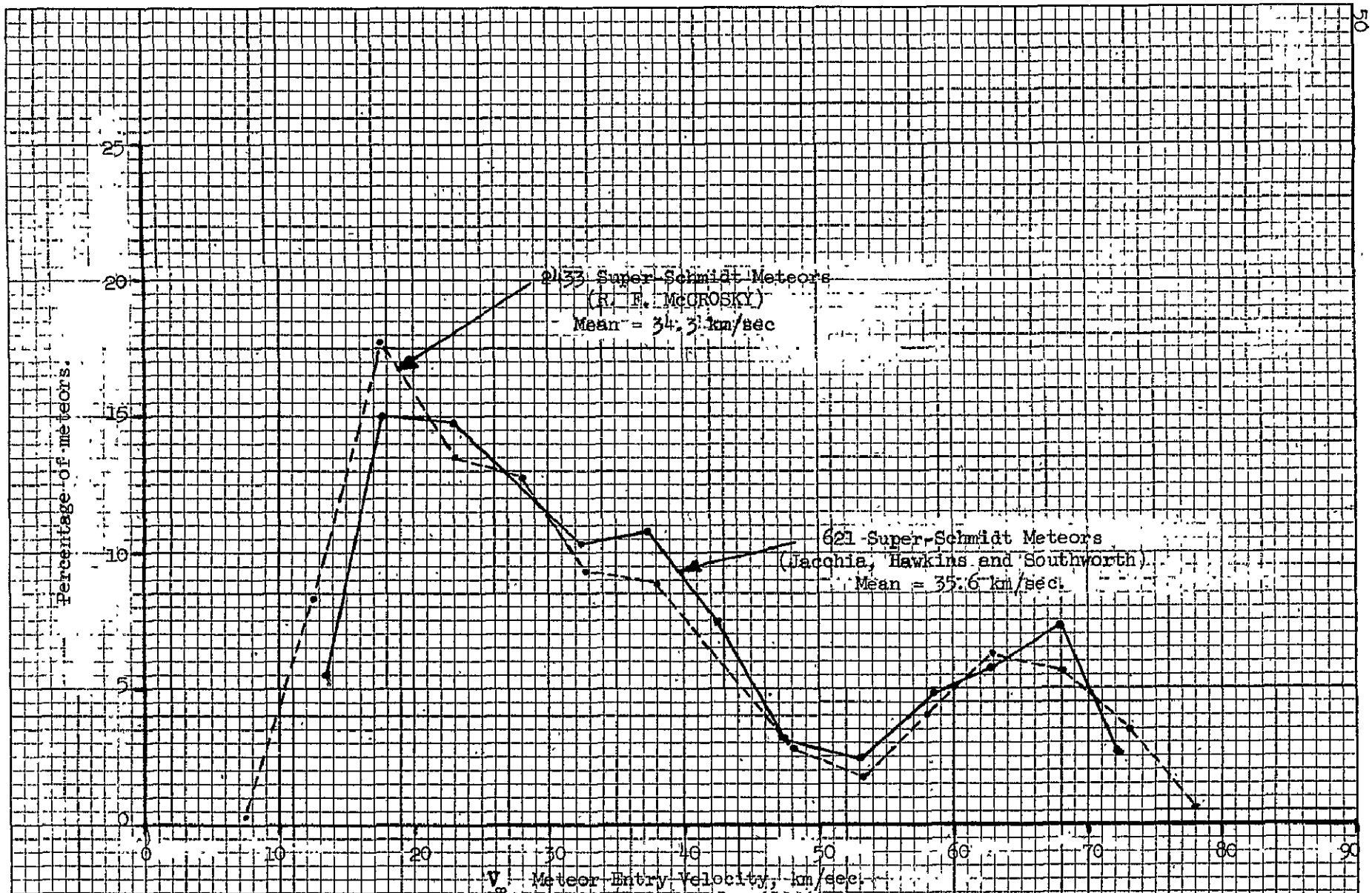

Figure 7.- Normalized distribution of photographic meteor entry velocities.

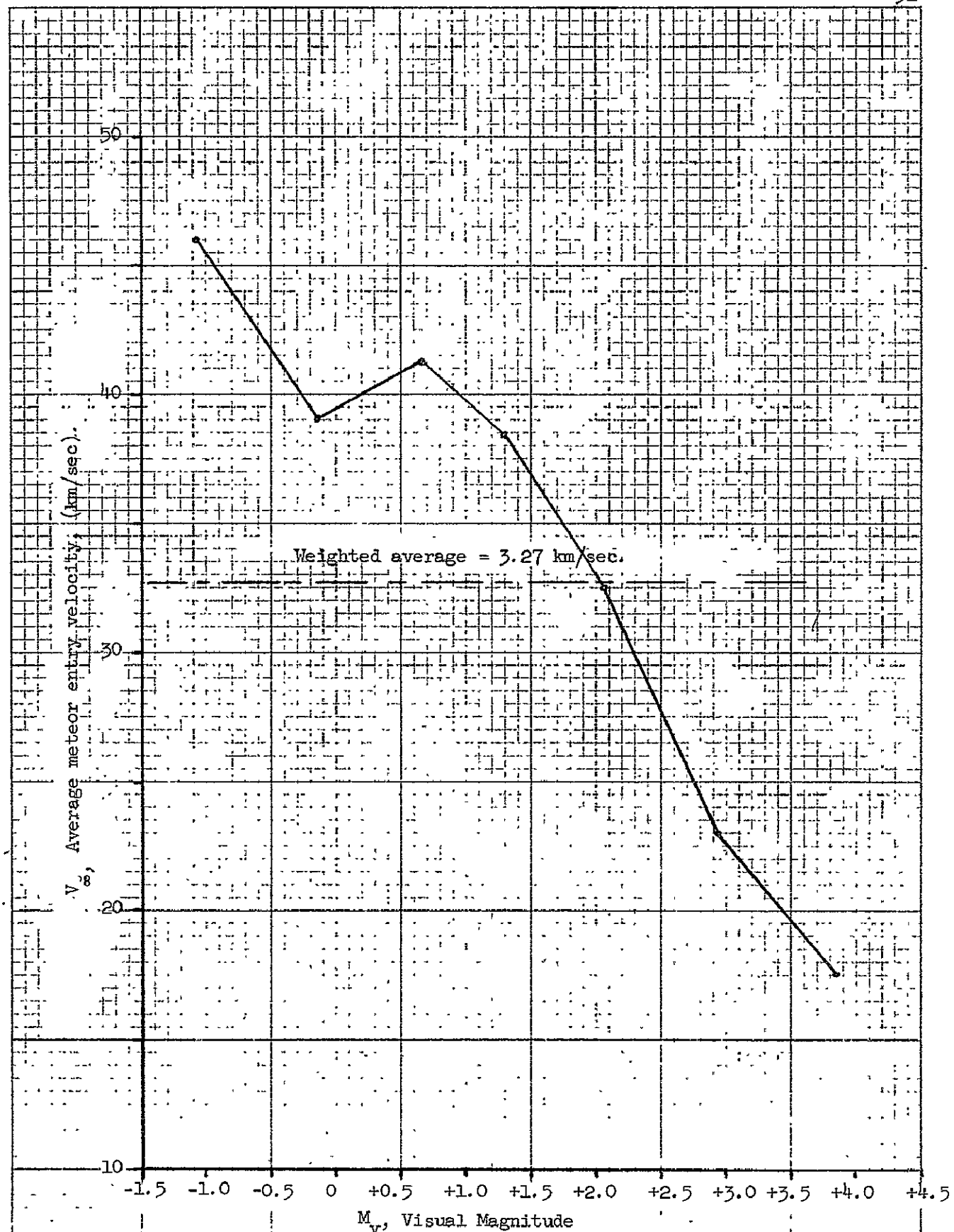

Figure 8.- Average velocity, V_∞ vs M_V, based on McCrosky's 2433 photographic meteors.

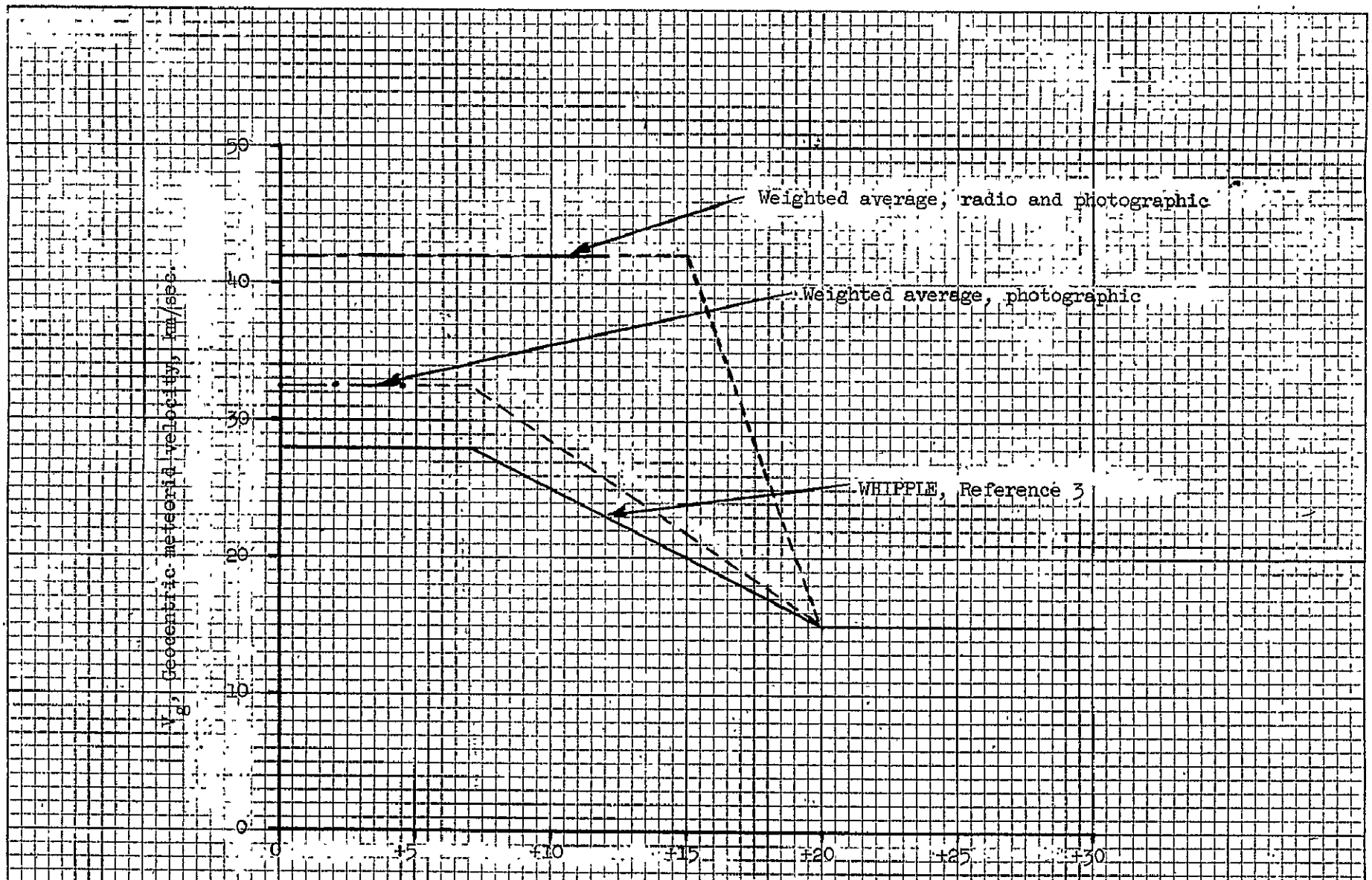

Figure 9.--Velocity vs magnitude.

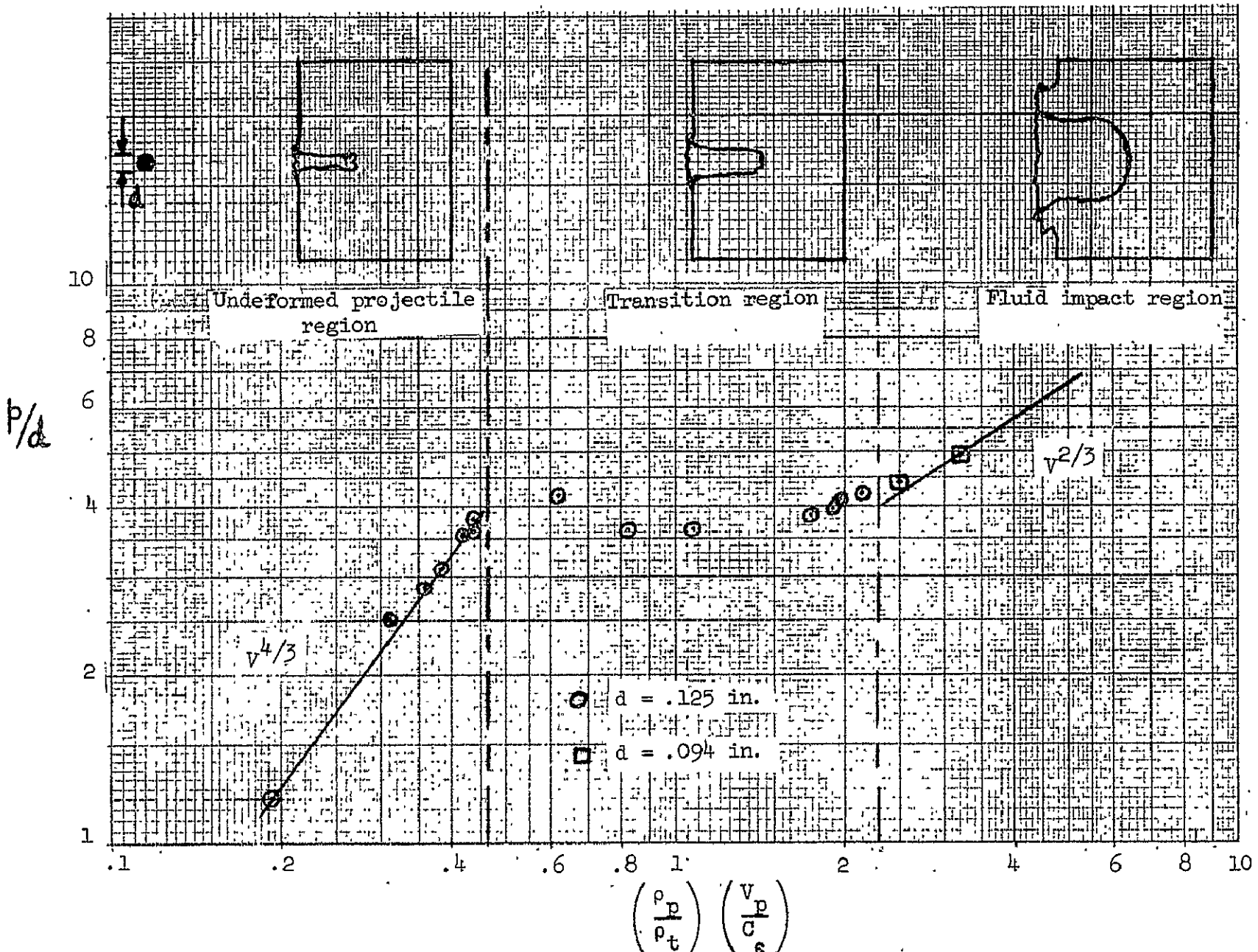

Figure 10.- Basic regions of impact as determined for tungsten-carbide spheres impacting lead targets.

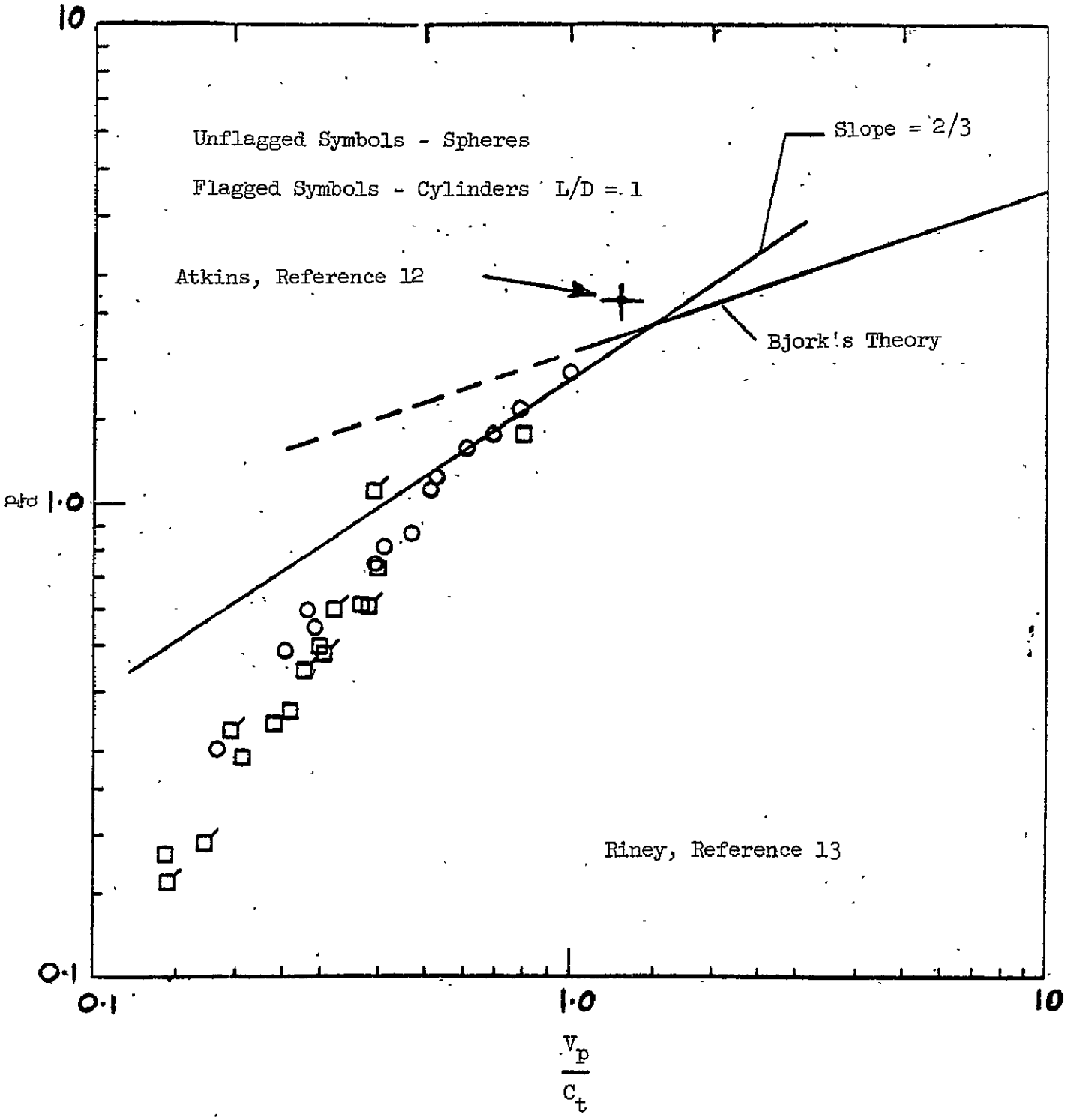

Figure 11.- Penetration parameters vs impact velocity for aluminum alloy target and projectile.

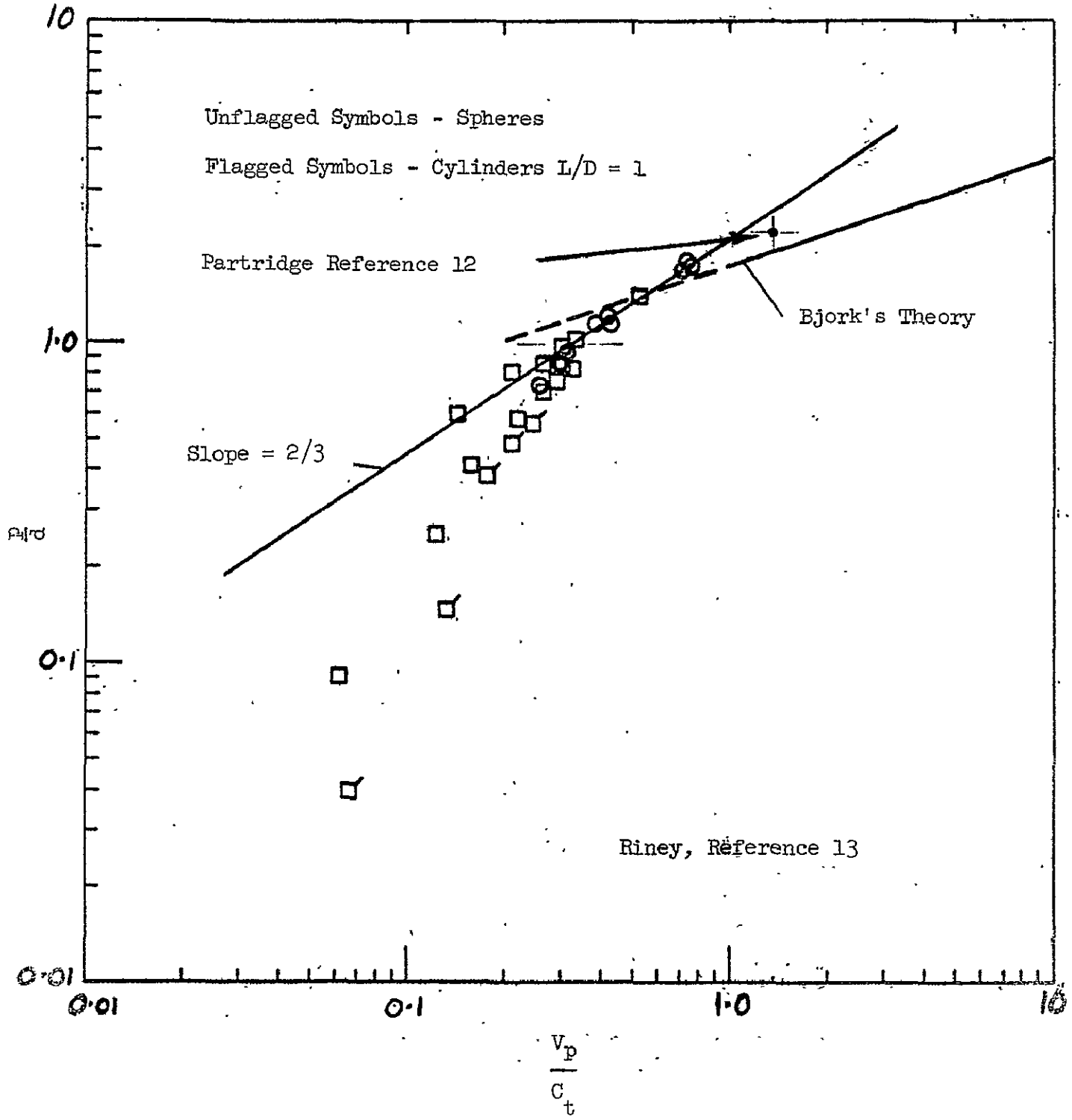

Figure 12.- Penetration parameter vs impact velocity for steel target and projectile.

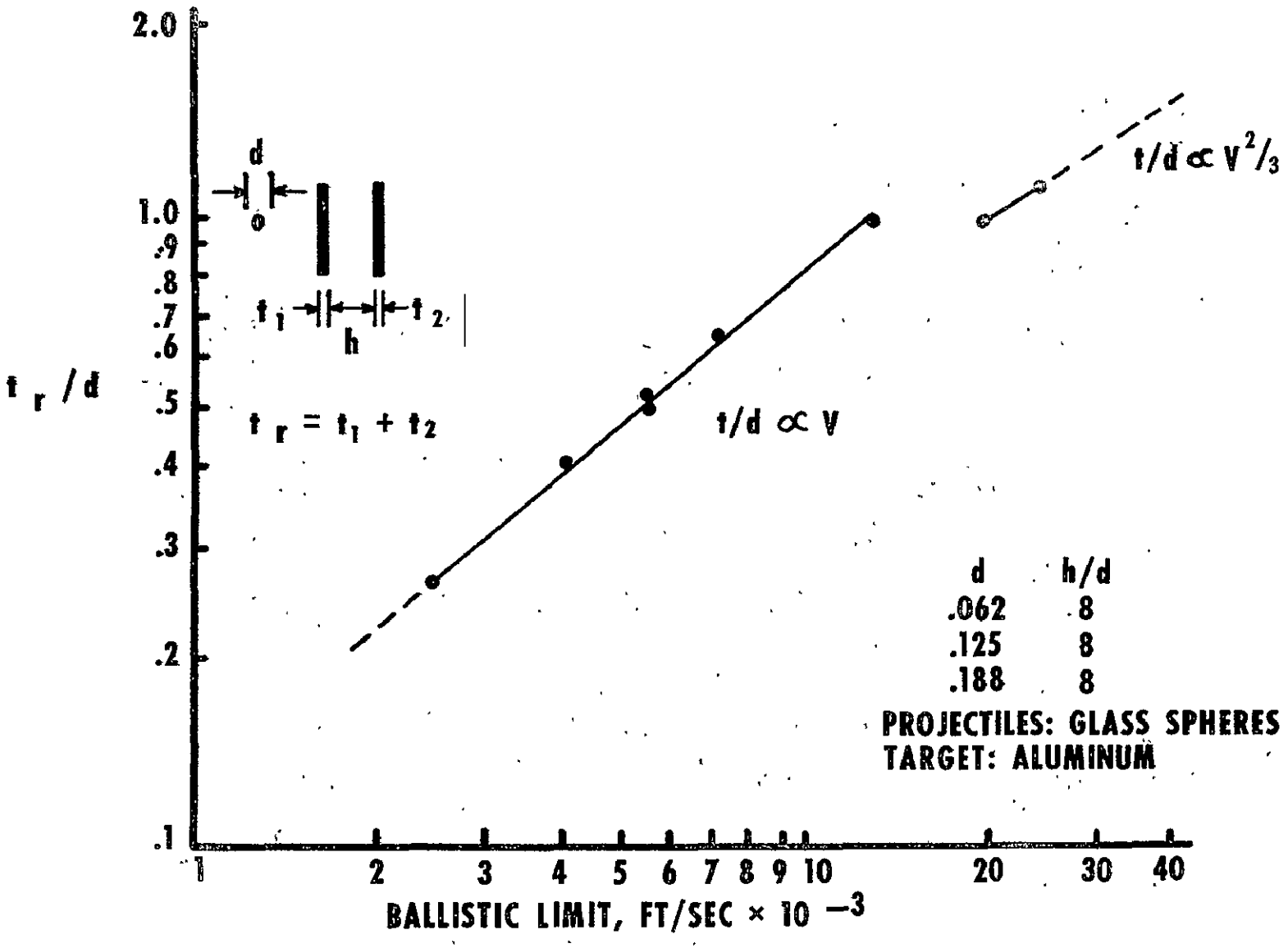

Figure 13.- Penetration parameter vs velocity for finite double-sheet targets.

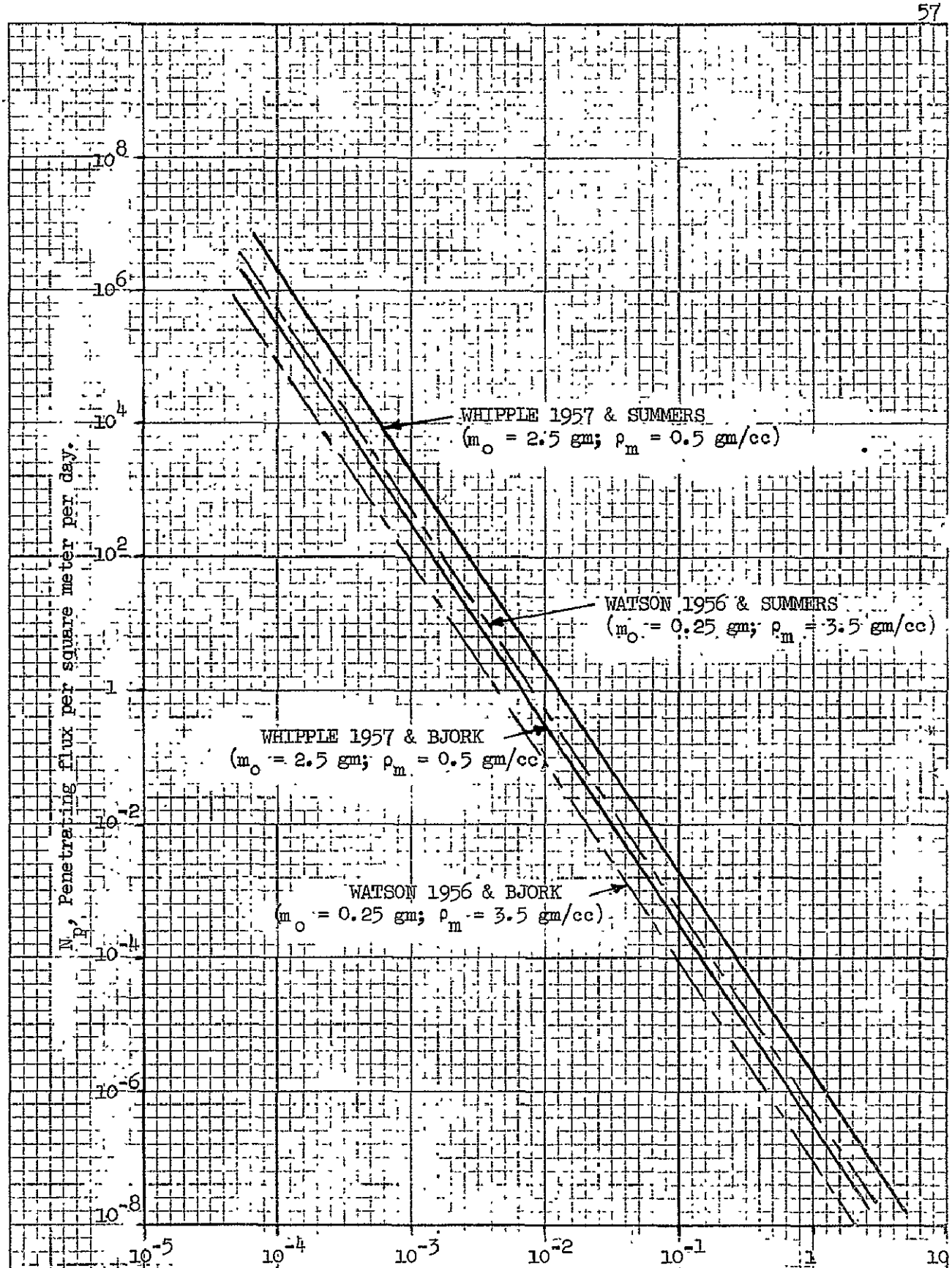

Figure 14.- N_p vs $\bar{t}$ for aluminum

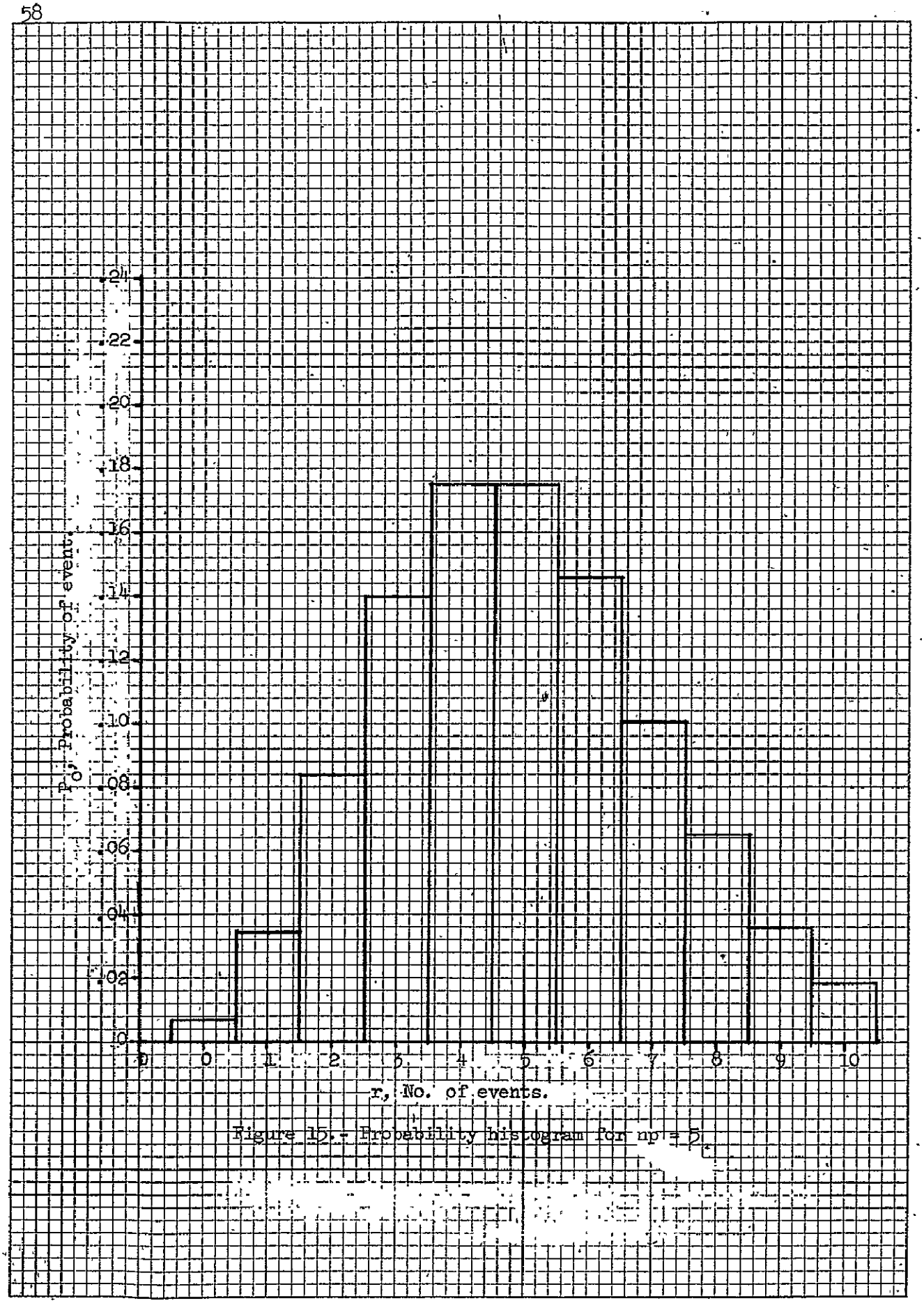

Figure 15.- Probability histogram for np = 5.

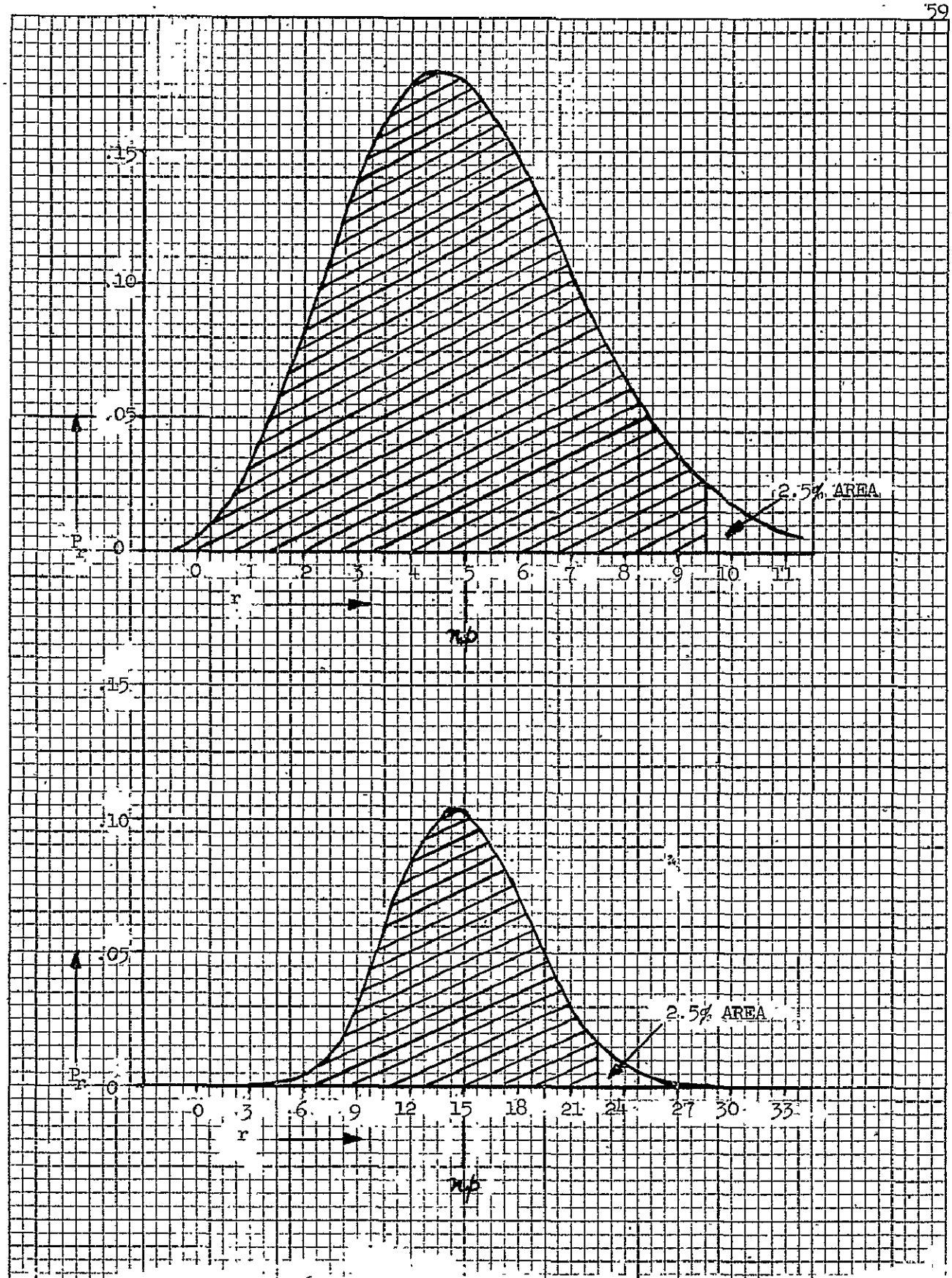

Figure 16.- Failure rate vs np for 97.5% area.

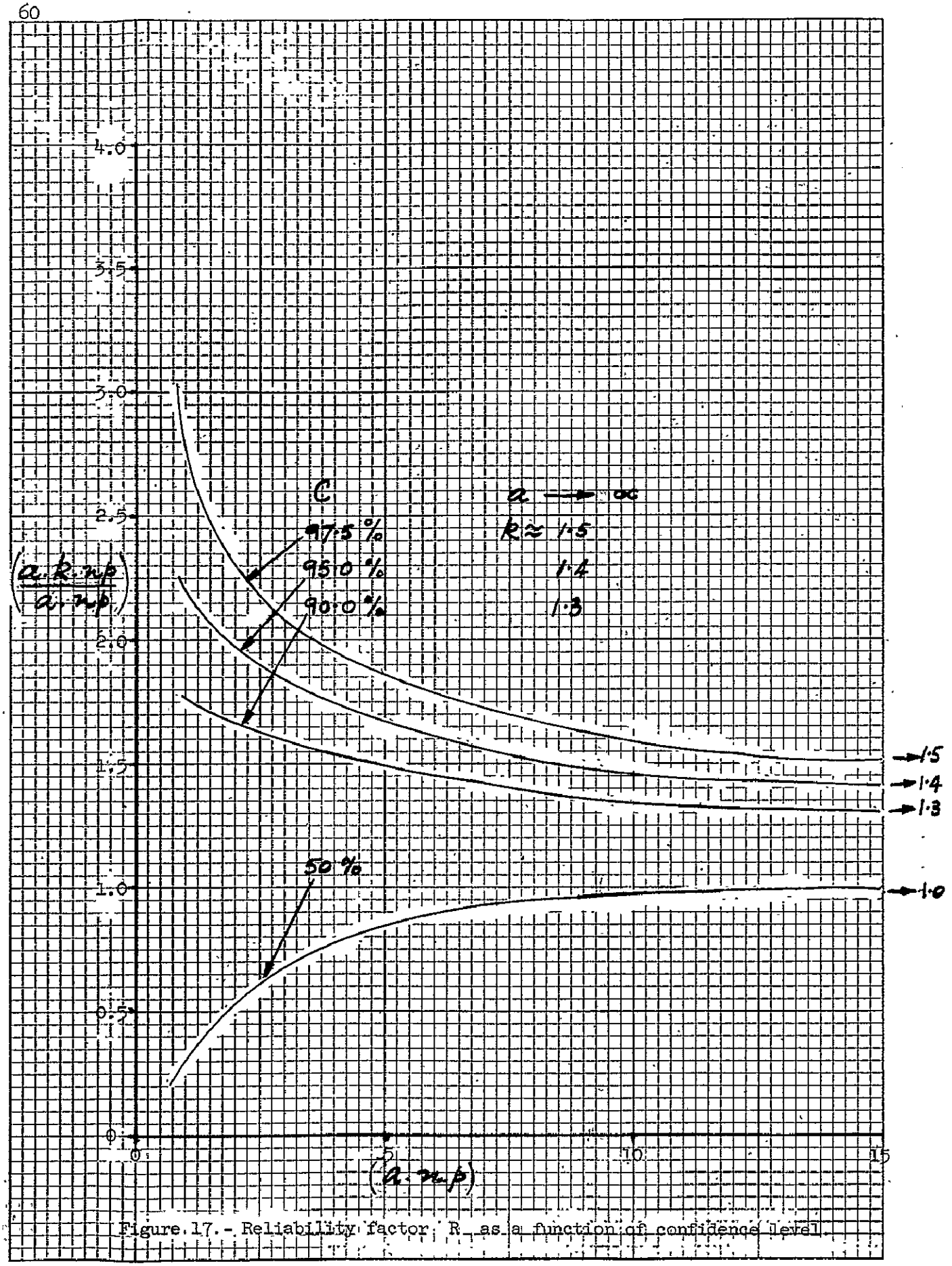

Figure 17.- Reliability factor, R, as a function of confidence level.

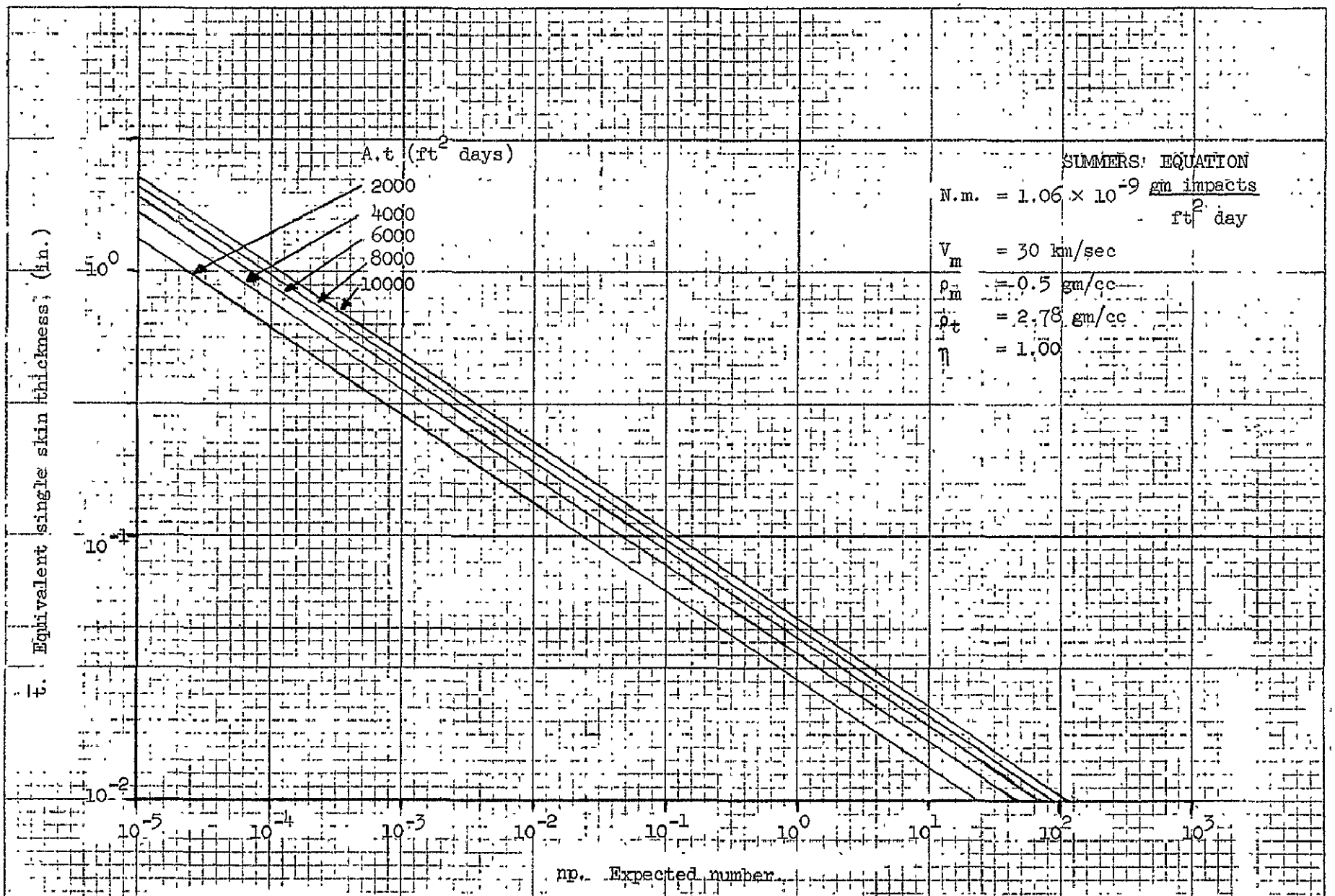

Figure 18.- np as a function of $\bar{t}$ based on Summers' equation.

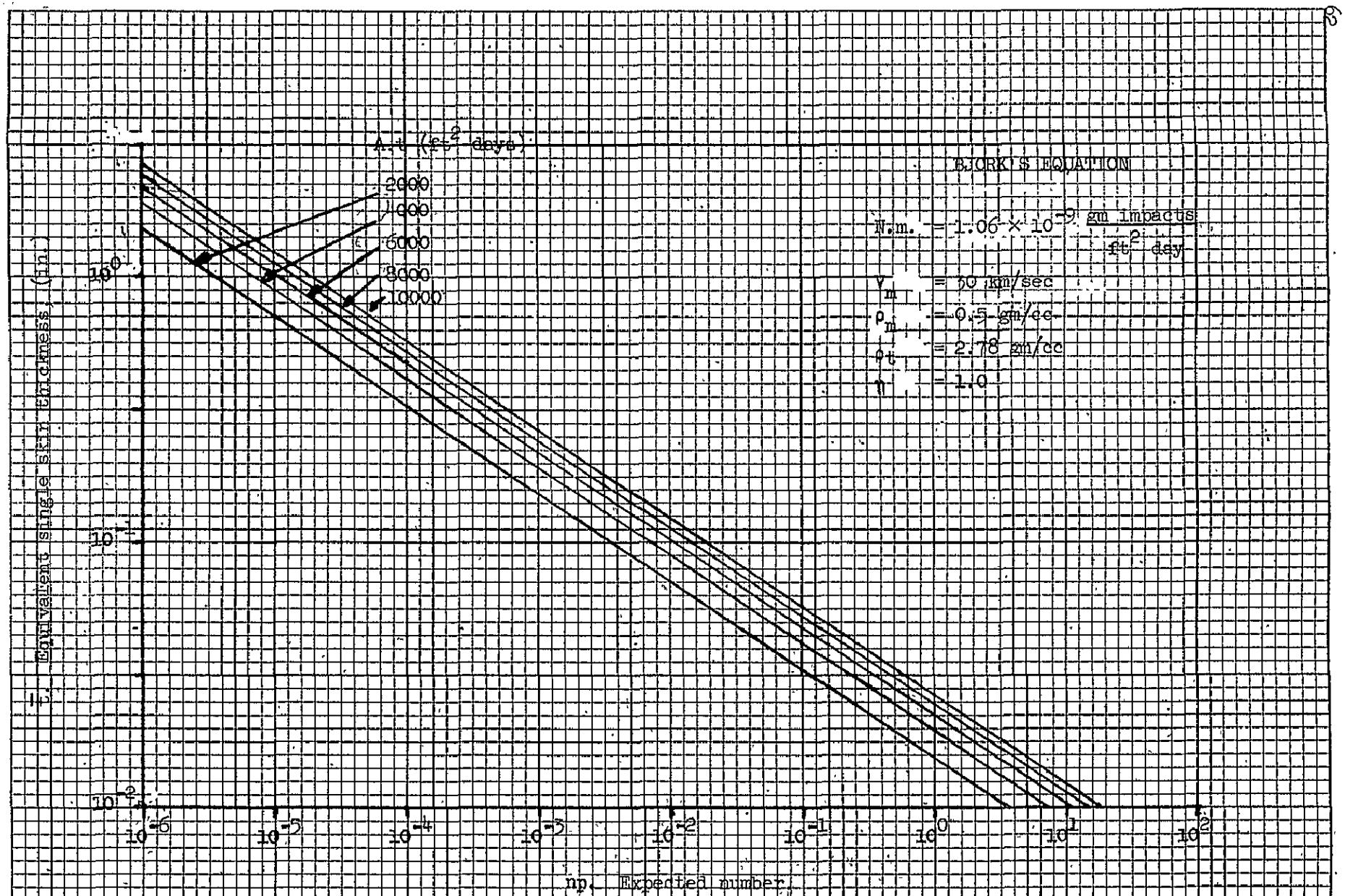

Figure 19.- np as a function of t based on Bjork's equation.

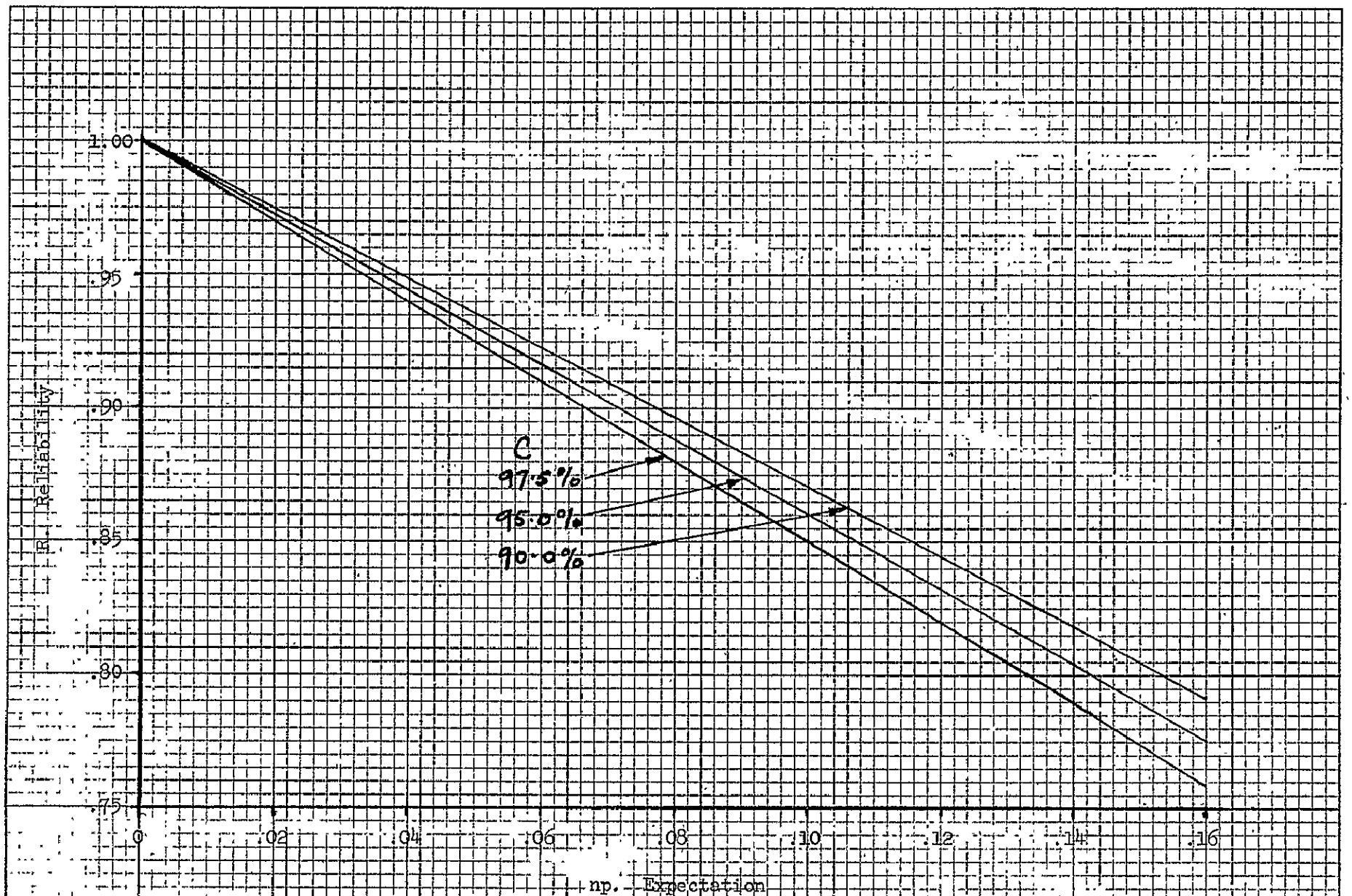

Figure 26.—R vs np as a function of confidence level.

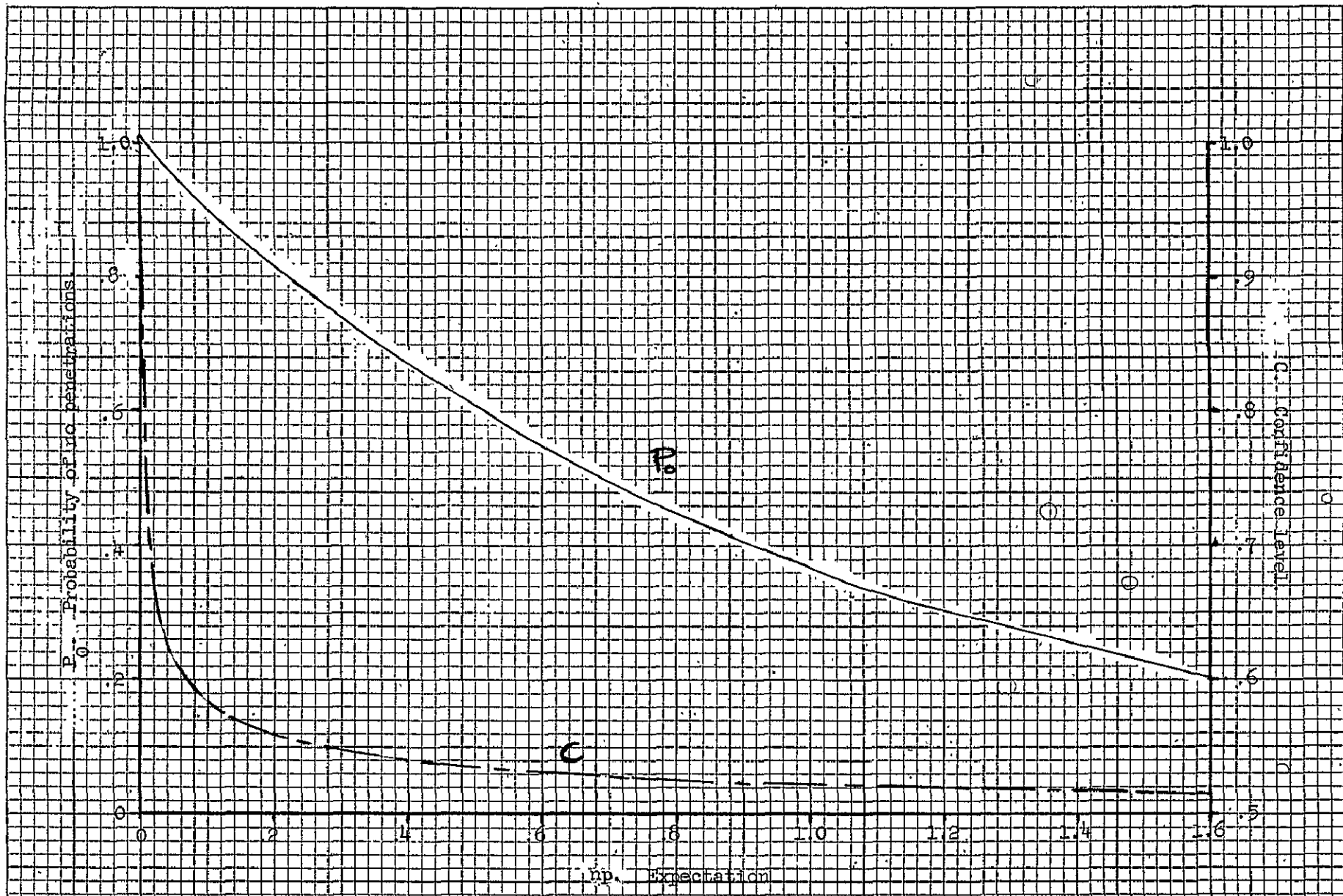

Figure 21.--Probability P_o vs np with corresponding confidence level.

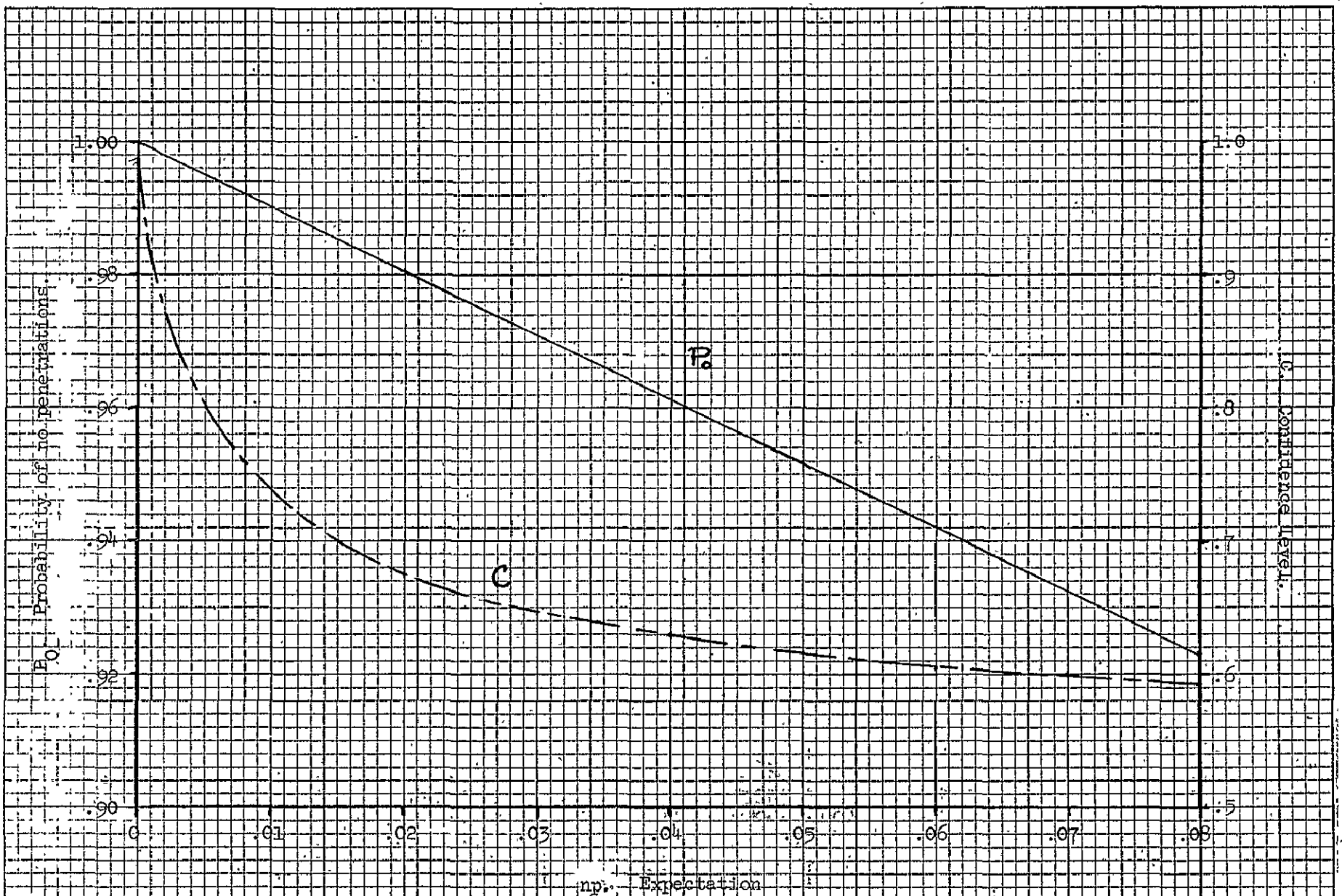

Figure 22.- Probability P_0 vs np with corresponding confidence level.

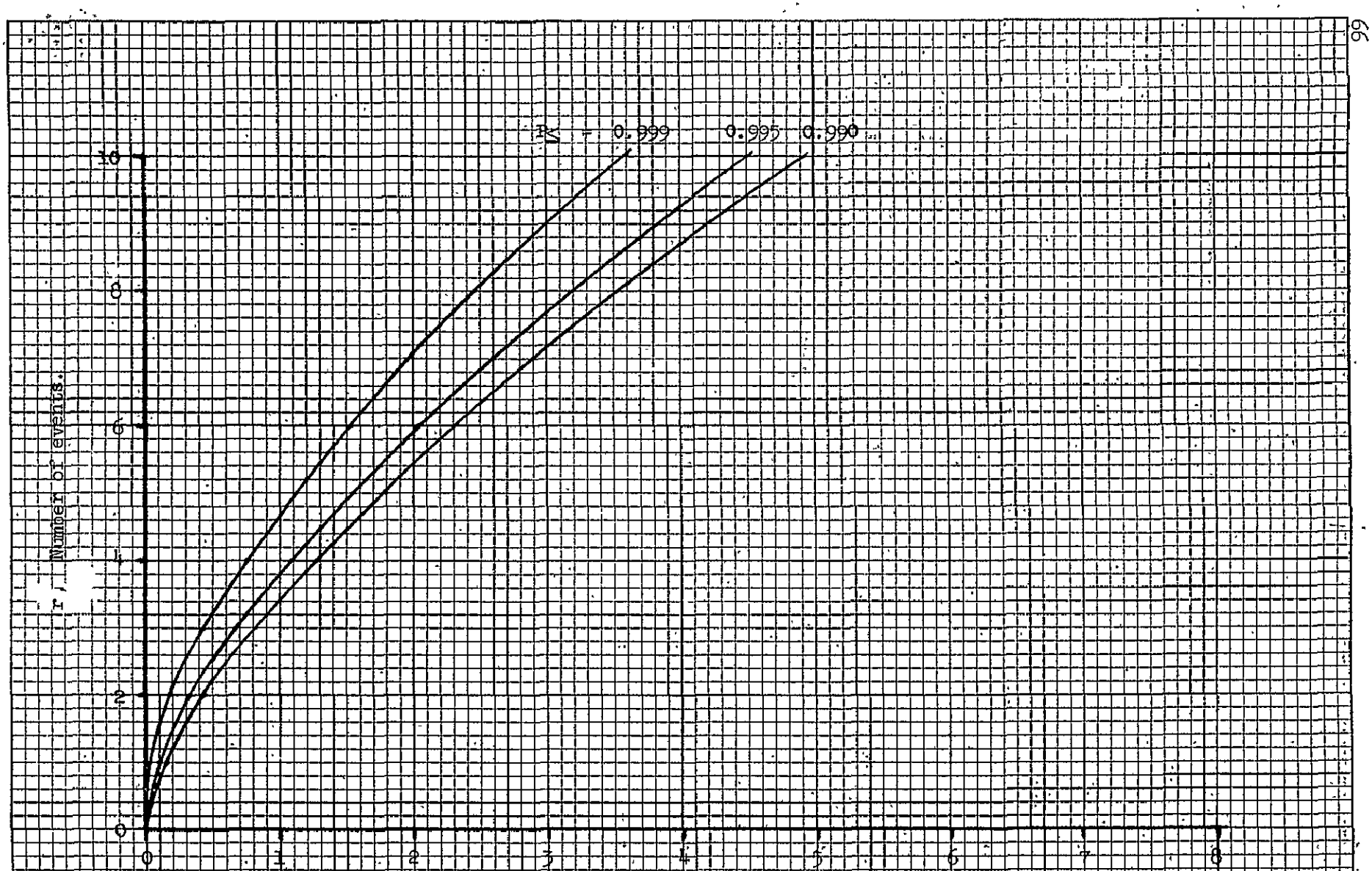

Figure 23.- Probability of no more than r events vs np.

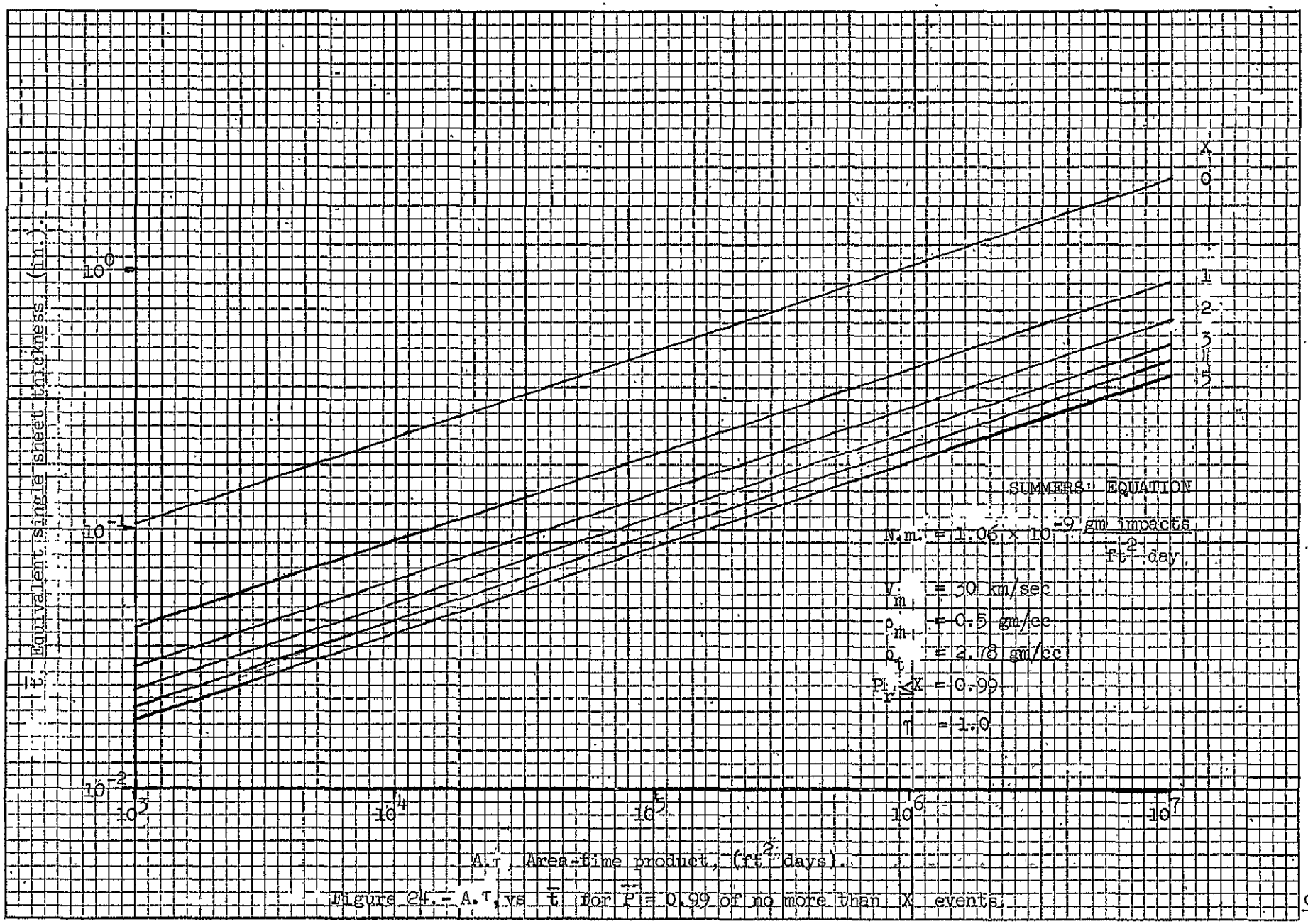

Figure 24.- $A.\tau$ vs $\bar{t}$ for $\bar{P} = 0.99$ of no more than X events.

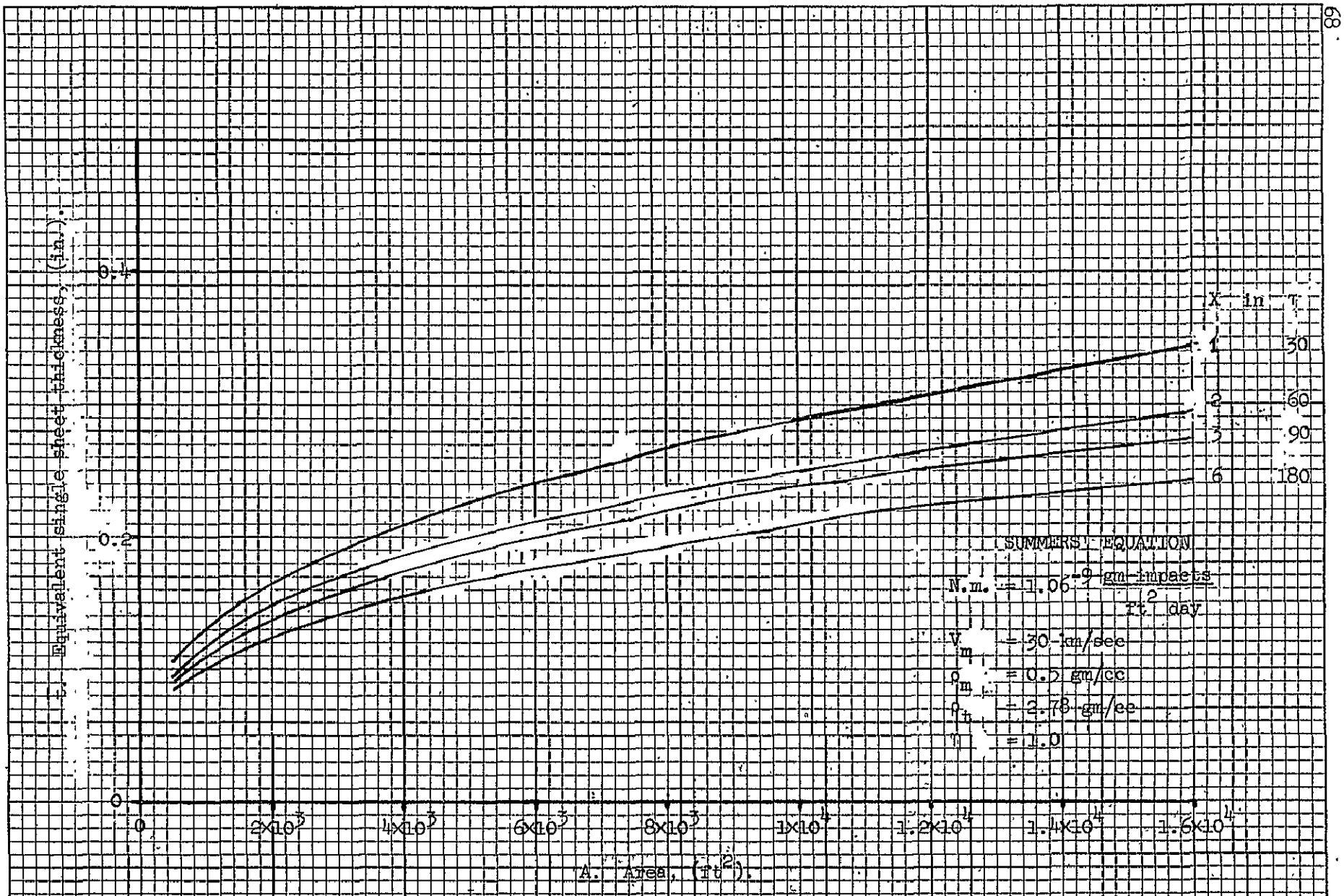

Figure 25.- A vs t for P = 0.99 of no more than X events in T days.